2007

Reduction of pertechnetate [Tc(VII)] by aqueous Fe(II) and the nature of solid phase redox products

John M. Zachara
Pacific Northwest National Laboratory, john.zachara@pnl.gov

Steve M. Heald
Pacific Northwest National Laboratory

Byong-Hun Jeon
Yonsei University

Ravi K. Kukkadapu
Pacific Northwest National Laboratory, ravi.kukkadapu@pnl.gov

Chongxuan Liu
Pacific Northwest National Laboratory

See next page for additional authors

Available online at www.sciencedirect.com
ScienceDirect
Geochimica et Cosmochimica Acta 71 (2007) 2137–2157
Geochimica et Cosmochimica Acta
www.elsevier.com/locate/gca

Reduction of pertechnetate [Tc(VII)] by aqueous Fe(II) and the nature of solid phase redox products

John M. Zachara [a,*], Steve M. Heald [a,c], Byong-Hun Jeon [b], Ravi K. Kukkadapu [a], Chongxuan Liu [a], James P. McKinley [a], Alice C. Dohnalkova [a], Dean A. Moore [a]

[a] *Pacific Northwest National Laboratory, Richland, WA 99354, USA*
[b] *Yonsei University, Kangwon-Do 220-710, Republic of Korea*
[c] *Argonne National Laboratory, Argonne, IL 60439, USA*

Received 19 April 2006; accepted in revised form 26 October 2006; available online 16 February 2007

Abstract

The subsurface behaviour of ^{99}Tc, a contaminant resulting from nuclear fuels reprocessing, is dependent on its valence (e.g., IV or VII). Abiotic reduction of soluble Tc(VII) by $Fe(II)_{(aq)}$ in pH 6–8 solutions was investigated under strictly anoxic conditions using an oxygen trap ($<7.5\times10^{-9}$ atm O_2). The reduction kinetics were strongly pH dependent. Complete and rapid reduction of Tc(VII) to a precipitated Fe/Tc(IV) form was observed when 11 μmol/L of Tc(VII) was reacted with 0.4 mmol/L Fe(II) at pH 7.0 and 8.0, while no significant reduction was observed over 1 month at pH 6.0. Experiments conducted at pH 7.0 with $Fe(II)_{(aq)} = 0.05$–0.8 mmol/L further revealed that Tc(VII) reduction was a combination of homogeneous and heterogeneous reaction. Heterogeneous reduction predominated after approximately 0.01 mmol/L of Fe(II) was oxidized. The heterogeneous reaction was more rapid, and was catalyzed by Fe(II) that adsorbed to the Fe/Tc(IV) redox product. Wet chemical and Fe–X-ray absorption near edge spectroscopy measurements (XANES) showed that Fe(II) and Fe(III) were present in the Fe/Tc(IV) redox products after reaction termination. ^{57}Fe-Mössbauer, extended X-ray adsorption fine structure (EXAFS), and transmission electron microscopy (TEM) measurements revealed that the Fe/Tc(IV) solid phase was poorly ordered and dominated by Fe(II)-containing ferrihydrite with minor magnetite. Tc(IV) exhibited homogeneous spatial distribution within the precipitates. According to Tc-EXAFS measurements and structural modeling, its molecular environment was consistent with an octahedral Tc(IV) dimer bound in bidentate edge-sharing mode to octahedral Fe(III) associated with surface or vacancy sites in ferrihydrite. The precipitate maintained $Tc(IV)_{aq}$ concentrations that were slightly below those in equilibrium with amorphous $Tc(IV)O_2{\cdot}nH_2O_{(s)}$. The oxidation rate of sorbed Tc(IV) in the Fe/Tc precipitate was considerably slower than $Tc(IV)O_2{\cdot}nH_2O_{(s)}$ as a result of its intraparticle/intragrain residence. Precipitates of this nature may form in anoxic sediments or groundwaters, and the intraparticle residence of sorbed/precipitated Tc(IV) may limit ^{99}Tc remobilization upon the return of oxidizing conditions.

1. INTRODUCTION

^{99}Technetium is a fission product of uranium-235 and plutonium-239 which poses a significant environmental hazard due to its long half-life ($t_{1/2} = 2.13\times10^5$ yr), abundance in nuclear wastes, and environmental mobility under oxidizing conditions. The Tc(VII) valence state is stable in oxic environments and exists as the pertechnetate anion [$Tc(VII)O_4^-$; (Wildung et al., 1979; Rard et al., 1999)] which is weakly sorbed by mineral material and forms few insoluble phases, with consequent high mobility in soil and groundwater. This form of ^{99}Tc is a risk-driving groundwater contaminant at some sites of nuclear reprocessing, such as the Hanford site in Washington State,

* Corresponding author. Fax: +1 509 376 3650.
E-mail address: john.zachara@pnl.gov (J.M. Zachara).

0016-7037/$ - see front matter © 2007 Elsevier Ltd. All rights reserved.
doi:10.1016/j.gca.2006.10.025

USA, and geochemical means are sought to reduce its mobility.

Tetravalent Tc [Tc(IV)] is the stable valence state under reducing or anoxic conditions (e.g., Eh < 0.1 V at pH 7). Tc(IV) readily forms a sparingly soluble ($10^{-8.2}$ mol/L), hydrated amorphous oxide precipitate [$Tc(IV)O_2{\cdot}nH_2O_{(s)}$; (Bondietti and Francis, 1979; Meyer et al., 1991; Burnett et al., 1995; Hess et al., 2004)], although carbonate complexation may enhance its solubility at higher pH depending on the alkalinity and $CO_{2(g)}$ pressure (Eriksen and Cui, 1991; Eriksen et al., 1993). The Tc(IV)/Tc(VII) couple bears similarity to the Cr(III)/Cr(VI) couple in terms of electron stoichiometry, oxyanion character of the higher valence state, and insolubility of the lower valence state [$\sim 10^{-7}$ mol/L for $Cr(III)(OH)_3$]. However, the chromium couple is more oxidizing:

$$Cr(VI)O_4^{2-} + 5H^+ + 3e^- = Cr(III)(OH)_3(s) + H_2O \quad E^o = 1.34\,V \tag{1}$$

$$Tc(VII)O_4^- + 4H^+ + 3e^- = Tc(IV)O_2 \cdot nH_2O(s) + (2-n)\,H_2O \quad E^o = 0.748\,V \tag{2}$$

Ferrous iron [Fe(II)] is an important reductant in anoxic sediments and groundwaters, and there is considerable interest in the reactivity of Tc(VII) with various Fe(II) forms because of the low solubility of the reduced state. Aqueous Fe(II) is reactive with $Cr(VI)O_4^{2-}$ (Eary and Rai, 1988; Buerge and Hug, 1997; Sedlak and Chan, 1997; Pettine et al., 1998; Wielinga et al., 2001) yielding a ferrihydrite-like, solid-solution product [$Cr_xFe_{1-x}(OH)_3$] that is less soluble than pure phase $Cr(III)(OH)_{3(s)}$ (Sass and Rai, 1987; Eary and Rai, 1988; Hansel et al., 2003a). In contrast, the homogeneous reduction of Tc(VII) by $Fe(II)_{aq}$, the subject of this paper, appears to proceed slowly or not at all, although the reaction is thermodynamically favourable in the circumneutral pH range (Cui and Eriksen, 1996a). Based on current understanding, the homogeneous redox reaction between Fe(II) and Tc(VII) can be written as follows under standard state conditions:

$$Tc(VII)O_4^- + 3Fe^{2+} + (n+7)H_2O = Tc(IV)O_2 \cdot nH_2O_{(s)} + 3Fe(OH)_{3(s)} + 5H^+ \tag{3}$$

with $\log K(298) = -13.5$ [using data from Rard et al. (1999)]. The component stoichiometry demonstrates that the thermodynamic feasibility of the redox reaction between $Fe(II)_{aq}$ and $Tc(VII)O_4^-$ is strongly determined by pH, Tc(VII) and $Fe(II)_{aq}$ activity, and the nature and activity of the resulting solid phase redox products [e.g., $Fe(OH)_{3(s)}$ is assumed for simplicity of reaction stoichiometry]. The dominant aqueous Fe(II) species is $Fe(H_2O)_6^{2+}$ in acidic/neutral solutions with pH < 7. This species was found to be an ineffective reductant for Tc(VII) over a reaction time of seven days in the only reported study of homogeneous Tc(VII) reduction by $Fe(II)_{aq}$ (Cui and Eriksen, 1996a).

Biological Tc(VII) reduction by dissimilatory metal reducing bacteria (DMRB) has been proposed for in situ remediation of Tc(VII)-contaminated subsurface environments in which Fe(III) oxides are in sufficient supply for DMRB growth and maintenance (http://www.lbl.gov/nabir/). The microbiologic reduction of Tc(VII) and associated Tc immobilization via precipitation has been investigated in the laboratory (Lloyd and Macaskie, 1996; Lloyd et al., 2000; Wildung et al., 2000; Liu et al., 2002) and field (Istok et al., 2004). The bioreduction of Fe(III) oxides by DMRB in anoxic soils and sediments produces biogenic Fe(II) (aqueous and mineral) that may also function as an indirect/abiotic reductant for Tc(VII) and other redox sensitive metals and radionuclides (Fitzpatrick et al., 1978; Lloyd et al., 2000; Wielinga et al., 2001; Hansel et al., 2003a; Fredrickson et al., 2004; Jeon et al., 2004b; Wildung et al., 2004; Burke et al., 2006a). Remaining unclear are the relative rates of biotic Tc(VII) reduction as compared to the potentially parallel abiotic reaction pathways of homogeneous and heterogeneous Tc(VII) reduction.

During experimentation on heterogeneous Tc(VII) reduction (Fredrickson et al., 2004) we observed unexpected losses of Tc(VII) from selected $Fe(II)_{aq}$–Tc(VII) controls. Follow-up research in this communication was performed to evaluate the potential for homogeneous Tc(VII) reduction by $Fe(II)_{aq}$under strictly anoxic conditions over a broader pH and concentration range than previously explored (Cui and Eriksen, 1996a). We observe that homogeneous reduction does occur at and above pH 7, and that the reaction evolves to a heterogeneous one with reaction progress. A sparingly soluble Fe/Tc precipitate is formed that is shown by X-ray absorption spectroscopy, Mössbauer spectroscopy, and transmission electron microscopy to have different characteristics than analogous ones resulting from homogeneous $Fe(II)_{aq}$–Cr(VI) reaction. The mixed Fe/Tc precipitate maintains low Tc(IV) aqueous concentrations and slows Tc(IV) oxidation. These results provide important insights on the biogeochemical cycling of Tc in seasonally anoxic environments and the geochemical behaviour of Tc in contaminated subsurface environments associated with nuclear fuels reprocessing facilities (e.g., the Hanford Site, Washington State, USA).

2. EXPERIMENTAL MATERIALS AND METHODS

2.1. Wet chemical experiments

2.1.1. Reduction

Experiments were conducted in 125 or 200 mL glass serum reaction bottles (referred to as master reactors). Syringes, needles, glass vials, and plastic tubes were used for sample processing. Glassware and plastic bottles were acid washed with 1% nitric acid, rinsed several times with distilled and de-ionized water (DDW), and purged with O_2–free Ar/H_2 (97:3) before use. Chemicals were reagent grade or better.

The reduction experiments were performed in a 97% Ar/3% H_2 atmosphere inside an anaerobic chamber (Forma Scientific, Marietta, OH) that was equipped with a palladium catalyst to remove trace O_2. Despite these precautions, it was discovered that the chamber contained up to 4×10^{-7} atm O_2 (corresponding to 0.29 ppm O_2 in the chamber atmosphere) (Jeon et al., 2004a). The presence of this trace amount of O_2 resulted in significant oxidation of Fe(II) in circumneutral pH solution. Consequently, all experiments with Fe(II) were conducted using

a low-temperature oxygen trap that is described elsewhere (Jeon et al., 2004a). Briefly, the O_2 trap consisted of bottles containing 0.90 mmol/L Fe(II) and 23.3 mmol/L Fe(III) as amorphous hydrous Fe(III) oxide (HFO). The pH was buffered at 8.1 with 0.1 M Tris(hydroxymethyl)-aminomethane (TRIS). The half-life for reduction of O_2 in the suspension phase of the oxygen trap was less than 0.5 s and the half-life for transfer of O_2 from the gas phase within the traps to the water phase was 6 min. The oxygen trap removed O_2 to strict anoxic conditions (i.e., $<7.5 \times 10^{-9}$ atm O_2) (Jeon et al., 2004a) and was able to maintain Fe(II) in pH 7 and 8 solutions for more than 2 weeks without any oxidation (Fig. 1).

DDW was purged with O_2–free Ar/H_2 overnight and stored in the chamber for preparation of all solutions and suspensions. Stock solutions of 0.25 and 0.025 mol/L Fe(II) were prepared in the chamber from chloride salt in 0.1 N HCl. These were stored in glass serum bottles that were wrapped in aluminum foil to exclude light. Isotopically enriched ^{57}Fe(II) stock solutions were also prepared in 0.1 N HCl from 96.7% pure ^{57}Fe(0) metal (Web Research Co., MN) following the procedure suggested by Williams and Scherer (2004). ^{99}Tc was purchased as $NH_4Tc(VII)O_4$ (Perkin Elmer Life Sciences Inc., Boston, MA) and diluted in DDW to produce a 5 mmol/L stock solution. The stock solutions and acid/base were stored in serum bottles and were extensively deoxygenated using the oxygen trap before addition to the master reactors. All samples that contained Fe(II) were kept inside the chamber. The solution pH in master reactors, which was varied from 6 to 8, was buffered using 10 or 30 mmol/L Na-1,4-piperazine *N*,*N*′-bis 2-ethanesulfonic acid (Na-PIPES). Solution pH was measured using an Orion 250A+ pH meter with a combination pH/temperature probe.

Degassed Na-PIPES buffer solution was added to the master reactors, and then the reactors were capped with thick butyl rubber stoppers and crimp sealed. The master reactors were deoxygenated with Ar/H_2 flowed through the oxygen trap using a syringe and needle. After 7 days of extensive de-oxygenation of the reactors, Fe(II) solution was added first and monitored for 4 days for all experimental conditions to ensure the stability of the added Fe(II) against any oxidation or precipitation. Tc(VII) was added to the master reactor, and dissolved Fe(II) and Tc(VII) concentrations were monitored over time. In some experiments, isotopically enriched ^{57}Fe(II) was added to enable Mössbauer spectroscopic measurements on the small quantities of precipitate that resulted from the redox reaction. The solution was continuously and gently stirred using a Teflon coated magnetic stirring bar at room temperature. The conditions of the reduction experiments are summarized in Table 1.

2.1.2. Oxidation

The Fe/Tc solid phase that was generated as a product in the reduction experiments was collected by centrifugation (10 min at 3000 rpm) at experiment termination and washed 3 times in the anaerobic chamber with deoxygenated 30 mmol/L Na-PIPES buffer solution at the desired pH (6.8, 7.0, and 8.0) to remove unreacted $Fe(II)_{(aq)}$. The solid was re-suspended in a sealed 50 mL Teflon centrifuge tube containing 25 mL deoxygenated 30 mmol/L Na-PIPES buffer solution. The suspension was subsequently oxygenated with compressed air that was bubbled through a water trap with a diffuser to saturate the air before entering the sample tube. The bubbling provided gentle mixing of the precipitate suspension. The kinetics of oxidative Tc(VII) dissolution were measured by monitoring dissolved Tc [presumed to be Tc(VII)] over time. The changes in solid/solution ratio due to sampling and evaporation were considered in the aqueous Tc(VII) calculation. The suspension pH changed by less than 0.05 pH unit during the oxidation experiment.

2.1.3. Wet chemical analytical techniques

Samples for dissolved Fe(II) were filtered (0.2 μm syringe filter) and 0.1–0.5 mL of the filtrate was added to 5 mL of ferrozine reagent (1 g/L ferrozine in 50 mmol/L Hepes buffer, pH 7.0) in the anaerobic chamber. After

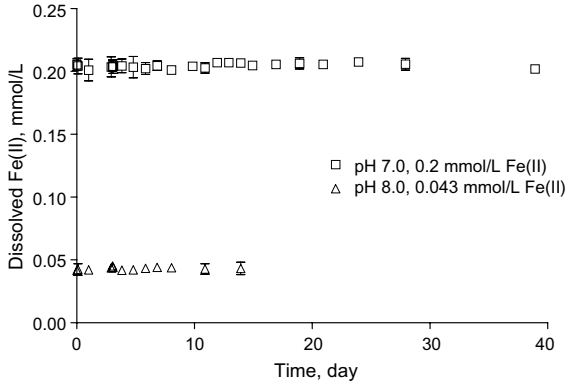

Fig. 1. Stability of $Fe(II)_{aq}$ in controls showing no oxidation for up to 40 days. The solutions were buffered by 10 mmol/L PIPES at pH 7 [0.2 mmol/L Fe(II)] and 8 [0.043 mmol/L Fe(II)]. Fe(II) was introduced to the reactors after 7 days of extensive de-oxygenation with the O_2 trap. Data represent means (±SD) of triplicate samples.

Table 1
Summary of experimental conditions and results

Reactor No.	pH	[Fe(II)][a] (mmol/L)	$Fe(OH)^{+}$[,b] (μmol/L)	E_H (V)	$t^{1/2}$[d] (day)
1	6.0 (±0.2)	0.4	0.09	0.028	NR[c]
2	6.8 (±0.1)	0.4	0.58	0.107	2.4
3	7.0 (±0.1)	0.05	0.12	0.073	22.7
4	7.0 (±0.1)	0.1	0.23	0.091	9.7
5	7.0 (±0.1)	0.2	0.46	0.109	3.1
6	7.0 (±0.1)	0.4	0.91	0.126	1.9
7	7.0 (±0.1)	0.6	1.37	0.137	0.90
8	7.0 (±0.1)	0.8	1.82	0.144	0.85
9	8.0 (±0.2)	0.4	8.90	0.225	<.25

[a] Added Fe(II).
[b] Combined concentration of both $Fe(OH)^{+}$ and $Fe(OH)_2{}^{o}{}_{(aq)}$ species calculated using MINTEQA2 (Allison et al., 1998).
[c] No apparent reaction.
[d] Experimental half-life for the overall reaction (homogeneous plus heterogeneous).

15 min, the samples were removed and the absorbance at 562 nm was determined with a Shimadzu UV-1240 spectrophotometer. Samples for dissolved Tc were filtered (0.2 μm) and 1 mL of the filtrate was added to 9 mL anoxic scintillation cocktail in the anaerobic chamber and ^{99}Tc concentration was analyzed with a Packard 2500TR liquid scintillation counter (Packard Instrument Co. Meriden, CT, USA). The 10-mL samples were each counted for 20 min. The PIPES buffer at different pH values without ^{99}Tc spike was also counted to determine the counting background and a minimum detectable ^{99}Tc concentration. Background counts in the unspiked buffer were pH independent and averaged ($n = 8$) 21.9 ± 0.903 dpm/mL. These background counts defined a minimum detectable ^{99}Tc concentration of $5.9 \pm 0.24 \times 10^{-9}$ mol/L. Aqueous Tc concentrations were calculated from the total counts in dpm/mL minus the background (21.9 dpm/mL).

2.2. Transmission electron microscopy (TEM)

Specimens for TEM analysis were prepared at the conclusion of the experiments (2–4 weeks) in the anaerobic chamber by applying 1 μL of suspension onto a 200 mesh Cu grid with a formvar support film coated with carbon. The solids were allowed to settle for 1 min, after which the clear liquid was gently blotted with a filter paper. The grid was dried in the anaerobic chamber. Imaging and analyses were performed using a JEOL 2010 High resolution TEM equipped with a LaB_6 filament operated at 200 kV with a nominal resolution of 1.8 Å. Images were digitally collected using a Gatan Digital Micrograph. Electron diffraction patterns were interpreted using JADE software (MDI, Livermore, CA). For comparison of specimen patterns with standards data, electron diffraction ring patterns were calculated from X-ray powder diffraction (PDF) data retrieved from a standards library (ICDD, 2003). The calculations were parameterized by fitting an electron diffraction pattern for sputtered gold (calculated from PDF 04-0784) to a sputtered gold pattern collected at the same time as the specimen patterns. The fitting was constrained by minimizing the difference between observed and theoretical d-spacings. The elemental composition of the precipitates was determined using the standard "semi-quantitative" data reduction software associated the instruments energy-dispersive spectroscopy (EDS) system (Oxford Instruments).

2.3. ^{57}Fe Mössbauer spectroscopy

Approximately 50 mL of pH 6.8, 7.0, 8.0 suspensions were filtered [0.2 μm pore-size (Millipore); 1.25 cm diameter] to collect the mineral product. The filter and associated solids were subsequently dried under strictly anoxic conditions and embedded within epoxy (ITW Performance Polymers, Rivera Beach, Florida) in a brass Mössbauer sample holder (0.95 cm by 1.27 cm). The sample holder was sealed with scotch tape and an oxygen impermeable polymer (aluminized Mylar stable to 4 K). The tape and polymer were snapped into the holder with rings made of carbonized-polyethyletherketone (PEEK) polymer to ensure a tight fit. The sample holders (Mössbauer disk) were stored in the anoxic chamber until analysis.

Mössbauer spectra were collected using a 50 mCi (initial strength) ^{57}Co/Rh source. The velocity transducer MVT-1000 (WissEL) was operated in a constant acceleration mode (23 Hz, ±12 mm/s). An Ar–Kr proportional counter was used to detect the radiation transmitted through the holder, and the counts were stored in a multichannel scalar (MCS) as a function of energy (transducer velocity) using a 1024 channel analyzer. Data were folded to 512 channels to give a flat background and a zero-velocity position corresponding to the center shift (CS or δ) of a metal iron foil at room temperature. Calibration spectra were obtained with a 25 μm thick α-Fe(m) foil (Amersham, England) placed in the same position as the samples to minimize any errors due to changes in geometry. A closed-cycle cryostat (ARS, Allentown, PA) was employed for 77 and 12 K measurements.

2.4. X-ray absorption (XAS) spectroscopy

2.4.1. Mineral, valence, and speciation standards

Various materials were used as reference phases for XANES and EXAFS analyses. Wustite (FeO), hematite (α-Fe_2O_3), and magnetite (Fe_3O_4) were obtained from commercial sources, while the preparation of other standards are described below.

Tc(IV)$O_2{\cdot}nH_2O$ precipitate was prepared by the reduction of Tc(VII) to Tc(IV) using sodium ditihionite ($Na_2S_2O_4$) inside a controlled atmospheric chamber (Hess et al., 2004). To reduce the Tc(VII) using the correct reductant to Tc(VII) ratio, 0.18 mL of 0.29 mol/L Tc(VII) was added to 4.12 mL of 0.195 mol/L $Na_2S_2O_4$. The pH was then adjusted to 12 using NaOH. A black precipitate quickly formed which was aged for 72 h. The precipitate was then washed 3 times using 20 mL of freshly prepared 0.01 mol/L $Na_2S_2O_4$ and then with anoxic deionzed water that had been scrubbed free of trace O_2 using the oxygen trap. The remaining solid was collected by filtration and then dried in an oxygen-scrubbed dessicator in the glove box.

A stock suspension of 2-line ferrihydrite ($5Fe_2O_3{\cdot}9H_2O$; 500 mmol/L) was prepared according to Cornell and Schwertmann (2000). The ferrihydrite suspension was allowed to age for 48 h inside the chamber. Excess Na and NO_3 were removed from the ferrihydrite by dialysis in deionized water. The ferrihydrite concentration was determined by gravimetric and Fe analyses. Aliquots were dried under anoxic conditions for XAS standards yielding 5–6 line ferrihydrite according to X-ray diffraction analysis.

A subsample of the Tc(IV)$O_2{\cdot}nH_2O$ precipitate (20 mg of ^{99}Tc) was added to 900 mL of 2 mol/L HCl and allowed to dissolve to steady state. The Tc(IV) solution was filtered through a 0.45-μm filter under anoxic conditions and the ^{99}Tc concentration quantified in the filtrate. A Tc(IV)/ferrihydrite coprecipitate reference phase with 1 mole % Tc(IV) was prepared by mixing a predetermined volume of acidic Tc(IV) solution with an appropriate volume of ferrihydrite suspension; this mixing lead to the dissolution of all of the ferrihydrite. The acidic Tc(IV)/Fe(III) solution

was then adjusted to pH = 7 (< 1 h) to form the coprecipitate. The resulting solid was aged for 2 h, washed with deoxygenated, deionized water, and dried under strictly anoxic conditions. The dried solid yielded an X-ray diffraction pattern of 2-line ferrihydrite with hints of a 6-line structure. The dried solid was subsequently dissolved in acid for quantitative analysis of Fe and Tc concentrations.

2.4.2. XAS methods

Extended X-ray adsorption fine structure (EXAFS) measurements were made at the Advanced Photon Source (APS) sector 20 beamlines, 20-ID and 20-BM on the Fe/Tc precipitates isolated from the pH 7.0 and pH 8.0 homogeneous reduction experiments by filtration and dried from ethanol in the anoxic glove box. A Si (1 1 1) monochromator was used with a 1-mm entrance slit located approximately 50 m from the source on both beamlines. The monochrometer allowed an energy resolution of about 1 eV at the Fe edge and about 4 eV at the Tc edge. The Fe edge measurements were made on beamline 20-BM using the dried Fe/Tc precipitates (or standards) that were mixed with vacuum grease or boron nitride. The samples were prepared and maintained under strictly anaerobic conditions using gases that were passed through the oxygen trap described in Section 2.1.1. The sample cells were sealed in teflon holders with two layers of Kapton. At the beamline, the reduced samples were kept under flowing nitrogen to avoid any oxygen diffusion through the Kapton. Data were taken in transmission mode with a Fe foil used for online energy calibration. The Fe edge was calibrated to better than 0.1 eV, allowing for an approximate error of 5% in the determination of Fe(II)/Fe(III) valence ratios based on near edge fits. The Tc(IV) standards [$Tc(IV)O_2{\cdot}nH_2O$; and Tc(IV) coprecipitated with ferrihydrite] were mixed with boron nitride in a sample holder and stored under anoxic conditions. These were also measured on 20-BM.

The Tc X-ray absorption measurements (XANES and EXAFS) were performed on the Fe/Tc precipitates that were embedded in epoxy for Mössbauer spectroscopy (Section 2.3). These were measured on beamline 20-ID in fluorescence mode using a 13-element Ge fluorescence detector. A total of 12 scans were run for each sample to improve the signal to noise ratio. A Mo foil was used for energy calibration.

The EXAFS and XANES data were analyzed using the Athena and Artemis interfaces to the IFEFFIT program package (Ravel and Newville, 2005). For the near edge analysis, the valence was obtained using linear combination fits of normalized standard spectra to the normalized data. Similar linear combinations fits were also made as appropriate for the EXAFS spectra. When more detailed modeling was required, theoretical models were calculated using FEFF 7 (Rehr and Albers, 2000) with the parameters refined using ARTEMIS.

3. RESULTS

3.1. Abiotic Tc(VII) reduction by Fe(II)

The use of the oxygen trap allowed us to synthesize and maintain solutions of $Fe(II)_{aq}$ and Tc(VII) that were functionally devoid of contaminant oxygen. The absence of contaminant oxygen was displayed by the long term stability of ferrous iron controls at pH 7 and 8 (Fig. 1), and the four day stability of $Fe(II)_{aq}$ solutions before spiking with Tc(VII) (Figs. 2 and 3b). The Tc(VII) solutions were presumed to be oxygen free by analogy because they were treated identically to those with only $Fe(II)_{aq}$. Thus, Tc(VII) was the only oxidant of consequence in the experiments with the Fe(II)–Tc(VII) mixtures.

The abiotic reduction of Tc(VII) was measured by its loss from solution. Reduction of Tc(VII) to Tc(IV) was rapid when 11 μmol/L of Tc(VII) was reacted with 0.4 mmol/L $Fe(II)_{aq}$ at pH 7.0, and almost instantaneous at pH 8.0 (Fig. 2). In contrast, no significant reduction was observed for up to 2 weeks of reaction time at pH 6.0. Extended monitoring of Tc(VII) in pH 6.0 solution for more than 1 month still showed no reaction. The data therefore verified that the reduction reaction was strongly pH dependent as shown in Eq. (3). Complete reduction of added Tc(VII) was observed within 1 h in a solution at pH 8.0, accompanied with the rapid decrease in dissolved $Fe(II)_{aq}$ from 0.40 to 0.36 mmol/L within 1 h and eventually to 0.33 mmol/L $Fe(II)_{aq}$ after 14 days of reaction time (Fig. 2b). Careful wet chemical analysis indicated that the total amount of $Fe(II)_{aq}$ loss from solution was higher than the

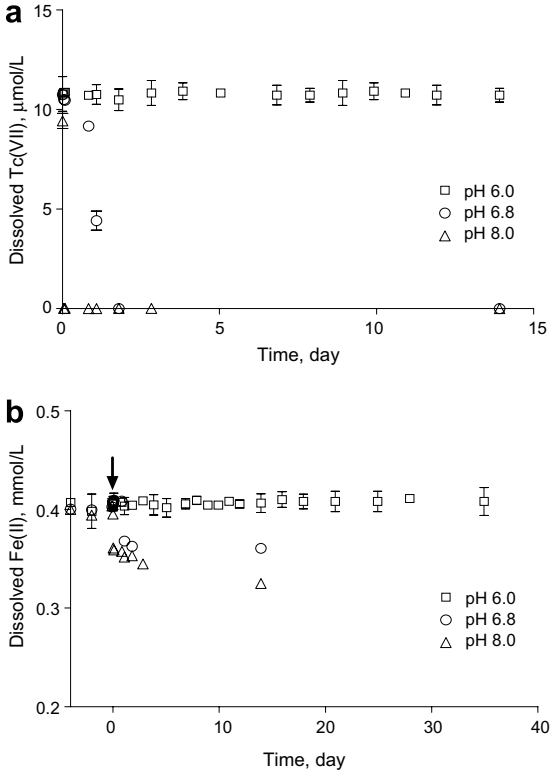

Fig. 2. (a) Abiotic reduction of Tc(VII) by $Fe(II)_{aq}$ and (b) recovery of added $Fe(II)_{aq}$ from the 10 mmol/L PIPES buffer solutions at different pH values. $[Tc(VII)]_{added} = 11$ μmol/L, and $[Fe(II)]_{added} = 0.4$ mmol/L. Data represent means (±SD) of triplicate samples. The arrow in (b) represents the time at which Tc(VII) was spiked into the $Fe(II)_{aq}$ solution.

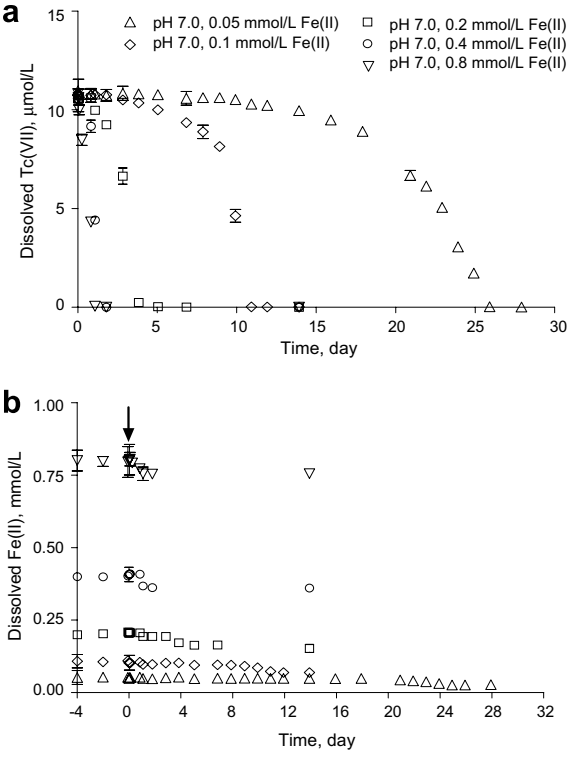

Fig. 3. (a) Abiotic reduction of Tc(VII) by $Fe(II)_{aq}$ and (b) recovery of added $Fe(II)_{aq}$ from the 10 mmol/L PIPES buffer solutions for different total Fe(II) concentrations at pH 7.0. $[Tc(VII)]_{added} = 11$ μmol/L, and $[Fe(II)_{aq}]_{added} = 0.05$–0.8 mmol/L. Arrow indicates time of Tc(VII) addition. Data represent means (±SD) of triplicate samples.

stoichiometric demand for complete reduction of Tc(VII) to Tc(IV) (Fe/Tc = 3; Table 2), implying sorption of $Fe(II)_{aq}$ by the solid phase product of the redox reaction (adsorption to or precipitation within). There was no significant change in pH in any of the experiments. Magnetite is thermodynamically the most stable iron phase given the experimental Fe(II)/Fe(III) ratio, solution composition, computed E_H (Table 1), and pH value (Jolivet et al., 1992; Tronc et al., 1992; Jeon et al., 2003). The reduction of Tc(VII) in pH 7.0 solution was completed within 2 days by 0.40 mmol/L $Fe(II)_{aq}$, and an excess in Fe removal from the aqueous phase was again observed.

Given the expected influence of $Fe(II)_{aq}$ concentration on the Tc(VII) reduction rate as implied by Eq. (3), experiments were performed over a range of Fe(II):Tc(VII) ratios at pH 7.0 (Fig. 3). The results obtained for the 0.05 mmol/L Fe(II) system were in good agreement with previous observations made by Cui and Eriksen (1996a), who found that Tc(VII) was stable for up to a week in solutions containing 0.04–0.07 mmol/L $Fe(II)_{aq}$ at pH 7. However, Tc(VII) was reduced at increasingly rapid rate as the $Fe(II)_{aq}$ concentrations increased. The reduction of Tc(VII) was complete after 1 day when $Fe(II)_{aq} = 0.8$ mmol/L. Moreover, the loss of Tc(VII) from solution showed complex kinetic behaviour in that the apparent reduction rate increased with reaction progress, accelerating markedly after the reduction of 1–2 μmol/L of Tc(VII). This phenomena was most evident for $Fe(II)_{aq} = 0.05$ and 0.1 mmol/L (Fig. 3a), but close inspection of the data showed its occurrence at higher $Fe(II)_{aq}$ concentrations as well. The reaction rate accelerated when solid-phase reaction products became evident as increased solution turbidity and the minor accumulation of dark sediment.

The final aqueous concentrations of ^{99}Tc were quantified in all experiments where Tc(VII) reduction proceeded to near completion [e.g., dissolved Tc(VII) ≈ 0 in Figs. 2 and 3a]. The results were independent of pH and Fe(II) concentration. The final, total counts averaged 35.0 ± 4.7 dpm/mL ($n = 18$). This value was above background (21.9 ± 0.903 dpm/mL) and yielded a background corrected concentration of 3.5×10^{-9} mol/L ($10^{-8.45}$ mol/L) of ^{99}Tc, presumed to exist as $Tc(IV)_{aq}$. The nominal solubility of $Tc(IV)O_2{\cdot}nH_2O_{(s)}$ at circumneutral pH is reported to be 6.3×10^{-9} ($10^{-8.2}$ mol/L) (Meyer et al., 1991; Rard et al., 1999; Hess et al., 2004).

Table 2
Elemental composition of the precipitates determined by wet chemical analysis

Reactor No.	pH	[Fe(II)] (mmol/L)	Fe (%)	Tc (%)	Fe/Tc
2	6.8	0.4	85.5	14.5	5.89
6	7.0	0.4	85.8	14.2	6.04
9	8.0	0.4	86.7	13.3	6.51

3.2. Kinetics and stoichiometry of Tc(VII) reduction

The homogeneous reduction of Cr(VI) by Fe(II) has been described as (Fendorf and Li, 1996; Sedlak and Chan, 1997; Pettine et al., 1998):

$$d[Cr(VI)]/dt = -k[Cr(VI)][Fe(II)]^n \quad (4)$$

where k is a function of Fe(II) speciation and increases with the presence of the hydrolyzed species $FeOH^+$ and $Fe(OH)_2^o$, and n is close to unity. Moreover, the rate behavior generally exhibits pseudo-first order decay {$d[Cr(VI)]/dt = -k_1[Cr(VI)]$; where $k[Fe(II)]^n = k_1$} for a given concentration of Cr(VI), Fe(II), and pH. Under pseudo-first order conditions, plots of $\ln[C_t/C_o]$ (where C_o is the initial concentration and C_t the concentration at time = t) versus time yield linear plots with slope of $-k_1$.

Pseudo-first order plots for the Tc(VII) reduction data in Figs. 2 and 3 demonstrated complex behavior as shown for 0.20 mmol/L Fe(II) at pH 7 (Reactor 5 data, Fig. 4a). Three regions were observed that were termed: (i) homogeneous reaction, (ii) heterogeneous reaction, and (iii) reaction completion. All of the kinetic data exhibited variants of this behavior. The homogeneous region ended at a dramatic breakpoint after which the reaction rate for heterogeneous reduction increased markedly. At pH 7, this breakpoint decreased in time with increased Fe(II) concentration, occurring at 23 d for 0.05 mmol/L Fe(II), 9 d for 0.1 mmol/L Fe(II), 3 d for 0.2 mmol/L, 1 d for 0.4 mmol/L, and 0.5 d for 0.6 mmol/L. The homogeneous region was not evident for 0.8 mmol/L Fe(II) at pH 7, or for the pH 8 data where Tc(VII) reduction was rapid. The breakpoints between the

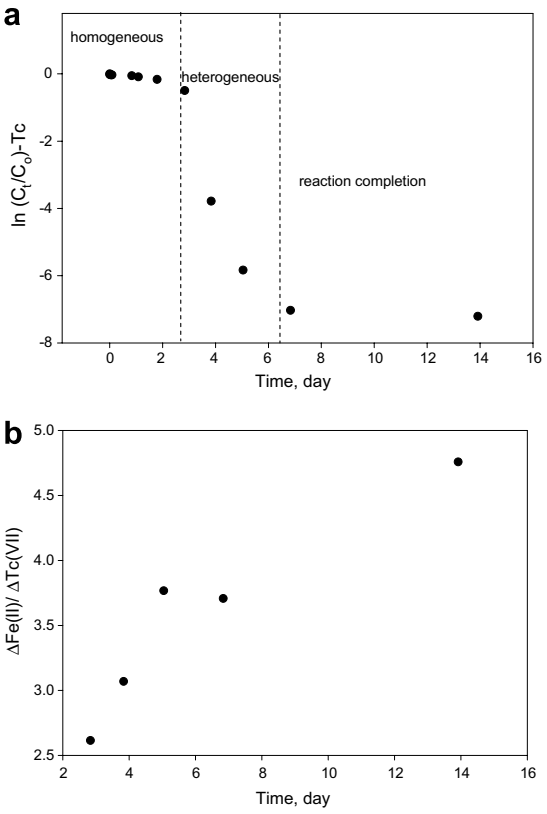

Fig. 4. (a) Pseudo-first order reaction plot for the reduction of 11 μmol/L Tc(VII), by 0.20 mmol/L Fe(II) at pH 7 (Reactor 5). Three reaction regions were evident as noted. The breakpoint between homogeneous and heterogeneous reduction intersected the y-axis (e.g., $t = 0$) at higher Fe(II) and pH values. (b) Apparent stoichiometry for the Tc(VII)–Fe(II) redox reaction in Reactor 5 as inferred by wet chemical analyses of the aqueous phase. Uncertainty in the ferrozine procedure and small changes in $[Fe(II)]_{aq}$ prevented stoichiometry calculations for time points before day 2.

homogeneous and heterogeneous regions, when observed, consistently occurred after 0.010–0.015 mmol/L of Fe(II) had been oxidized by Tc(VII) reduction. Plots of $\ln[C_t/C_o]$ versus time for the homogeneous region data were slightly to markedly curvilinear, indicating lack of overall conformance to pseudo-first order behavior. An exception was the pH 7, 0.05 mmol/L Fe(II) experiment where the homogeneous region was linear ($r^2 = 0.869$) yielding $k_1 = 0.005$ (± 0.0005) day^{-1}.

The stoichiometry of the redox reaction was difficult to asses for the homogeneous region because the small changes in Fe(II) concentration were within the variance of the ferrozine-Fe(II) analytical procedure. Reaction stoichiometry as determined by aqueous phase Tc(VII) and Fe(II) analyses was analytically accessible during the heterogeneous phase because of greater reaction progress (Shown for Reactor 5 in Fig. 4b). Consistent with Reaction 3, an approximate 3:1 Fe(II)/Tc(VII) loss ratio was observed for all experiments at the early stages of heterogeneous reduction. This ratio increased to over 4 following reaction completion as Fe(II) sorbed to and reacted with solid-phase products of the redox reaction.

3.3. Characterization of the reduced Fe/Tc product

The results of the wet chemical experiments indicated that the $Fe(II)_{aq}$–Tc(VII) solute mixtures were free of trace contaminant oxygen and that the changes in the aqueous concentration of the two solutes were a consequence of the direct electron transfer reaction between them. The redox reaction yielded a solid-phase product containing insoluble Fe and Tc(IV). The electron stoichiometry of the redox reaction [Eq. (3)] implied that the precipitates would exhibit a Fe:Tc ratio of 3, but higher ratios were observed (Table 2, Fig. 4b). The precipitate was ferrimagnetic (at least in part) as it was collected by stir bars in the reaction vessels indicating the presence of magnetite or maghemite. The solids were dark-brown to black in color. Significant efforts were expended to characterize the solid phase reaction products in order to more accurately define the overall redox reaction defined conceptually by Eq. (3).

3.3.1. Transmission electron microscopy

Precipitates obtained from reaction vessels at pH 6.8, 7.0, and 8.0 were analyzed by transmission electron microscopy. Solids from multiple experiments were analyzed at pH 7.0 and 8.0 to assess potential variations in product character between replicated experiments, and none were observed. The precipitates from pH 7.0 and pH 8.0 were virtually identical in all respects. They consisted of loosely connected, 30–50 nm particle aggregates arranged in chain or "sponge-like" morphology (Fig. 5). The individual aggregates were themselves comprised of tightly packed 5–10 nm crystallites (Fig. 5b) that exhibited distinct lattice fringes (Fig. 5c). Precipitates obtained from the pH 6.8 experiment exhibited different morphology from those at higher pH. Approximately 63% of the precipitate mass existed in the form of 50 nm aggregates comprised of tightly packed, <3 nm particles (Fig. 6a). The remainder (~37%) was present in the form of more crystalline, somatoidal structures up to 50 nm long (Fig. 6b), that exhibited distinct lattice fringes (Fig. 6c). These structures were similar to nascent hematite formed from ferrihydrite (Fischer and Schwertmann, 1974).

SAED patterns were measured on over thirty locations in the pH 6.8, 7, and 8 samples. These ranged from common diffuse patterns characteristic of poorly crystalline materials (~75% of the patterns), to less common distinct diffraction banding indicative of crystalline materials (~25% of the patterns). The patterns collected for the more crystalline material were virtually identical for all three pH samples indicating the presence of a common, single phase. In the most well-defined of these patterns (Fig. 7a and b), six d-spacings were observed: 0.245, 0.215, 0.164, 0.144, 0.126, and 0.120 nm. These spacings well matched rings calculated from the reference powder diffraction file of magnetite (PDF file 19-0629) and overlain on Fig. 7a, specifically corresponding to d-spacings at 0.253–0.242, 0.210, 0.162, 0.142, 0.128–0.127, and 0.121 nm. Diffraction patterns for 6-line ferrihydrite (PDF file 29-0712; Fig. 7b) did not show agreement with the sample data, except at the largest d-spacings. Similar comparisons were made between many other Fe oxides (hematite, goethite, akaganeite, maghemite,

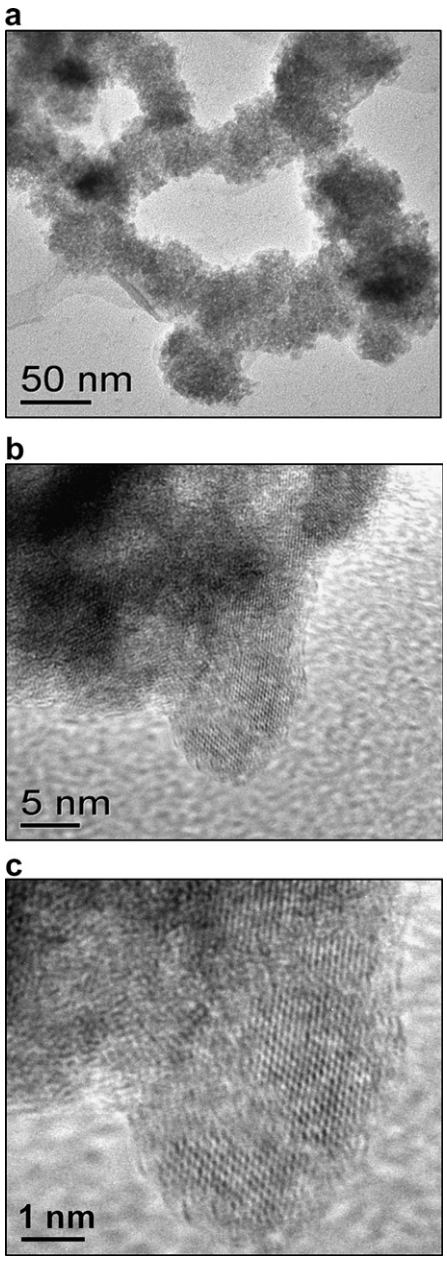

Fig. 5. Transmission electron micrographs of the pH 7.0, Fe/Tc precipitate at increasingly small scale.

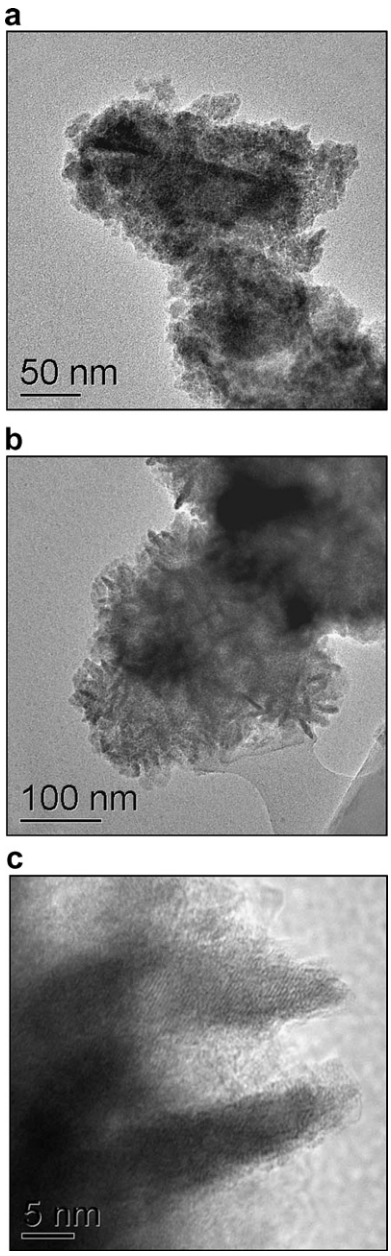

Fig. 6. Transmission electron micrographs of the pH 6.8, Fe/Tc precipitates: (a) tightly packed <3 nm particles, (b) larger ''somatoid-like'' crystallites, and (c) detail of somatoids.

titanomagnetites) and Tc compounds, with only synthetic feroxyhite (PDF file 13-0087) and maghemite (PDF file 25-1402) providing partial matches to the observed rings that were inferior to that observed for magnetite.

The chemical compositions of the precipitates were mapped by EDS at different spatial scales ranging from >100 nm to <5 nm. The Fe:Tc atomic ratio was found to be the same at all spatial scales in the pH 7 and 8 samples, indicating a chemically homogeneous precipitate without distinct areas of Tc localization. Analyses around crystallite peripheries showed no evidence for the concentration of Tc on mineral surfaces, with Fe:Tc atomic ratios identical to the bulk. Slight variations in composition were observed in spot analyses at <10 nm, but all analyses yielded average Fe:Tc composition values of 86(±0.5):14(±0.5) atomic %. The pH 6.8 samples were also homogeneous at different spatial scales, although spot analyses at the 5 nm scale showed a slight difference in Fe:Tc composition between the fine grained aggregates (86.1%:13.9%) and the somatoidal precipitates (85.0%:15.0%), $n = 6$ for each. This difference was consistent between measurements, but was near the limit of precision for EDS data reduction, and so may not be significant. The compositional results were consistent with those from wet chemical analyses (Table 2).

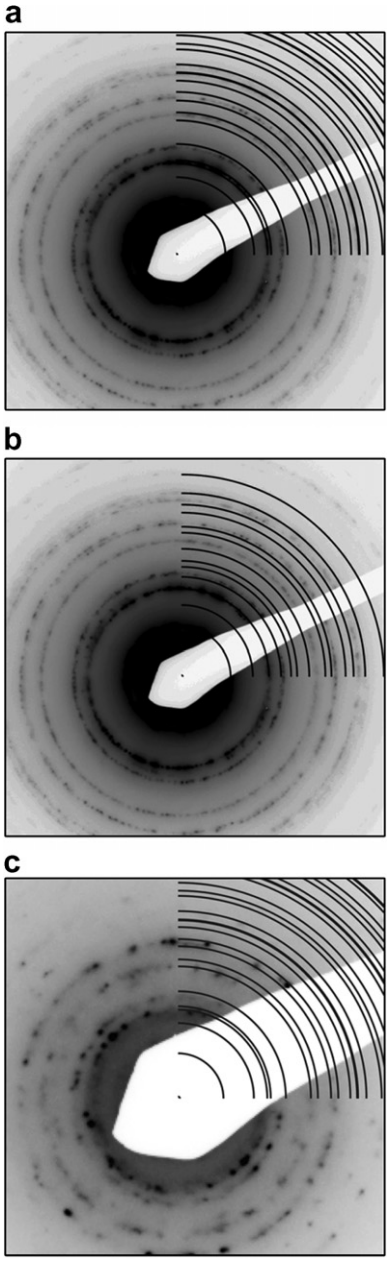

Fig. 7. Selected area electron diffraction (SAED) of (a) pH 8 Fe/Tc precipitate with calculated diffraction rings of magnetite (PDF #19-0629), (b) same sample pattern, but with computed lines of ferrihydrite (PDF #29-0712), and (c) oxidized pH 8 Fe/Tc precipitate with computed lines of magnetite (PDF #19-0629).

3.3.2. XANES and EXAFS spectroscopy

XANES analyses revealed that the average Fe valence for the Fe/Tc samples was below that of Fe(III) (Fig. 8a). Using FeO and hematite as standards, average valences of 2.85 [15% Fe(II)] for the pH 7 and 2.75 [25% Fe(II)] for the pH 8 Fe/Tc precipitates were determined from linear combination fits of the edge region. A similar analysis for magnetite yielded an average valence of 2.63 [37% Fe(II)] that was close to, but slightly lower than the expected value of 2.67 [33% Fe(II)]. The Fe valence measurements suggested that significant residual $Fe(II)_{aq}$ in the wet chemical experiments adsorbed to and reacted with the initial Fe(III)/Tc(IV) product of the redox reaction to yield a mixed valence Fe(III)–Fe(II)/Tc precipitate.

Both magnetite and maghemite (γ-Fe_2O_3) have a combination of tetrahedral and octahedral Fe sites, while only octahedral sites exist in ferrihydrite ($5Fe_2O_3{\cdot}9H_2O$) and hematite (α-Fe_2O_3). These differences in coordination environment affect the small pre-edge feature at 7113 eV (Fig. 8a). For symmetric octahedral bonding as found in ferrihydrite (primarily) and hematite the feature is strongly suppressed. Debate has persisted on the presence of tetrahedral Fe(III) in ferrihydrite (Eggleston and Fitzpatrick, 1988; Zhao et al., 1994) which exhibits a small pre-edge feature. For magnetite, a phase whose presence was implied in the Fe/Tc precipitates by SAED (Fig. 7a), the feature is stronger due to the tetrahedral sites and distortion in the octahedral sites. An increase in the pre-edge feature above that observed for ferrihydrite and consistent with the presence of magnetite/maghemite was noted for the two Fe/Tc precipitates (Fig. 8a), suggesting the possibility of some tetrahedral Fe bonding in the redox products.

The extended fine structure for Fe in the Fe/Tc precipitates [$\chi(k)$ data in Fig. 9a] bore strong similarity to our standard of 6-line ferrihydrite, with the suggestion of a contribution from stoichiometric magnetite especially in the pH 8 sample. The average Fe environment for the magnetite and maghemite structures is quite similar, and as a consequence it was not possible in our EXAFS data analyses to discern preference for either structure. Because of evidence for the presence of magnetite in the Fe/Tc precipitates from SAED (Section 3.3.1), we presumed that magnetite was the primary source of tetrahedral Fe bonding in the samples. The χ(k) data were consequently fitted to linear combinations of ferrihydrite and magnetite. The EXAFS spectra of the pH 8 sample was well fitted with 11% magnetite and 89% ferrihydrite (Fig. 9b). Similar fitting for the pH 7 sample yielded 100% ferrihydrite, with the suggestion of the presence of a small amount of an additional non-magnetite component (data not shown).

The near edge Fe spectra for Fe/Tc samples were fitted using a similar linear combination approach. In this fitting, it was assumed that magnetite was the sole contributor of Fe(II) to the near edge spectrum. Modeling of the sample near edges (Fig. 8b) yielded significantly higher magnetite contents then obtained from EXAFS: 62% magnetite/38% ferrihydrite for the pH 8 sample (Fig. 8b), and 25% magnetite/75% ferrihydrite for the pH 7 sample (data not shown). Accepting the results of the EXAFS fitting as a reasonable phase and structural model of the samples, the contrasting results of the XANES fitting implied that the ferrihydrite contained significant Fe(II). Using the EXAFS fitted phase distributions as a constraint, we computed Fe(II) contents of 20.6% and 15% in the ferrihydrite of the pH 8 and pH 7 samples, respectively.

The Tc near edge spectrum for both of the Fe/Tc precipitates was virtually identical to nanometer-sized, poorly crystalline $TcO_2{\cdot}nH_2O$, indicating Tc(IV) valence (data not shown). The absence of Tc(VII), which forms rapidly in presence of oxygen, indicated success in our sample

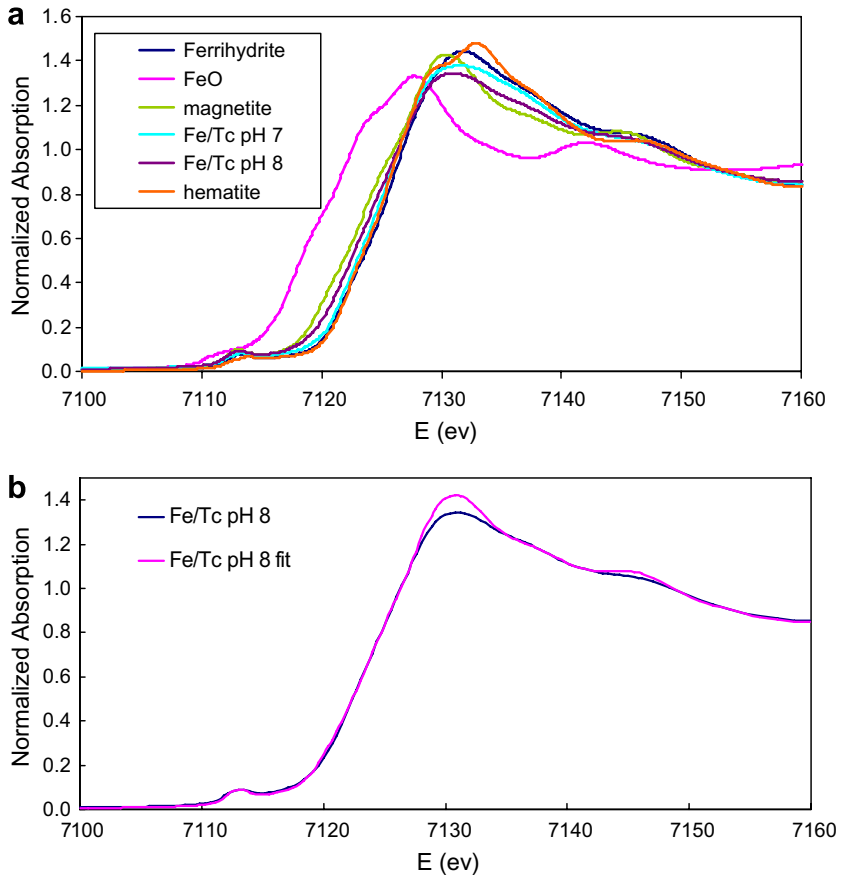

Fig. 8. (a) Fe-XANES spectra of the pH 7 and pH 8 Fe/Tc precipitates as compared to ferrous oxide [Fe(II)O], magnetite [$Fe(II)Fe(III)_2O_4$], hematite [α-$Fe(III)_2O_3$], and ferrihydrite [$5Fe(III)_2O_3{\cdot}9H_2O$], and (b) results of linear combination fitting of the pH 8 sample data with 62% magnetite and 38% ferrihydrite.

preservation efforts. The Tc-EXAFS data were quite similar for the redox products at both pHs (Fig. 10a). These, in turn, were significantly different from that of $TcO_2{\cdot}nH_2O$, but were virtually identical to our reference sample of Tc(IV) that was coprecipitated with ferrihydrite (Fig. 10a).

A number of models were applied to the EXAFS data to determine the Tc(IV) coordination environment. The first shell was well fit with 6 oxygen neighbors, regardless of model. The outer shell distances, however, were inconsistent with the extended edge sharing, Tc(IV)-octahedral chain model as described by Lukens et al. (2002) and recently applied to Tc(VII) reaction products with environmental reductants (Maes et al., 2004), as the second shell transform peak was strongly suppressed from that expected for multiple Tc second-shell neighbors. The extended distances also did not agree with Tc(IV) substitution in magnetite-like octahedral sites.

Because of the close similarity of the pH 7 and 8 EXAFS data with the Tc(IV)-ferrihydrite precipitate, and the dominance of ferrihydrite in the precipitate as implied by Fe-EXAFS fitting (e.g., Fig. 9b), we evaluated whether the Tc-EXAFS spectrum was consistent with Tc(IV) adsorption to, or substitution within ferrihydrite. This evaluation began with the development of a ferrihydrite structural model to describe the Fe-EXAFS spectrum of the 6-line ferrihydrite standard (Fig. 9a). A conceptual ferrihydrite structural model to guide these calculations was abstracted from Drits et al. (1993), Janney et al. (2000a,b), Jansen et al. (2002). This model contained numerous different Fe sites (up to 12) because of the defected and disordered ferrihydrite structure. FEFF calculations on these sites indicated that they exhibited some similar characteristics: (i) a split first shell, (ii) two or more separate second shell Fe neighbors, and (iii) a range of third shell O neighbors. Under the assumption that Fe site occupancy in ferrihydrite averaged 0.5, the following structural model was abstracted from the conceptual model and used to fit the ferrihydrite Fe-EXAFS data: 3 short and 3 long O first shell bonds, 3 short and 3 long Fe second shell bonds, and 3 short and 3 long O third shell bonds. This structural, two Fe-shell model gave good fit to the ferrihydrite Fe-EXAFS data (Fig. 9c) with reasonable coordination numbers, bond distances, and fit statistics (Table 3). The model was therefore considered a reasonable, but not unique representation of the structural environment of Fe in ferrihydrite.

The Tc-EXAFS data could also be explained within context of the ferrihydrite model. Our first modeling attempt embedded a symmetric TcO_6 octahedron (Tc–O = 2.00 Å) in the defected ferrihydrite structure in a bidentate, edge-sharing configuration with an octahedral FeO_6 site. A key

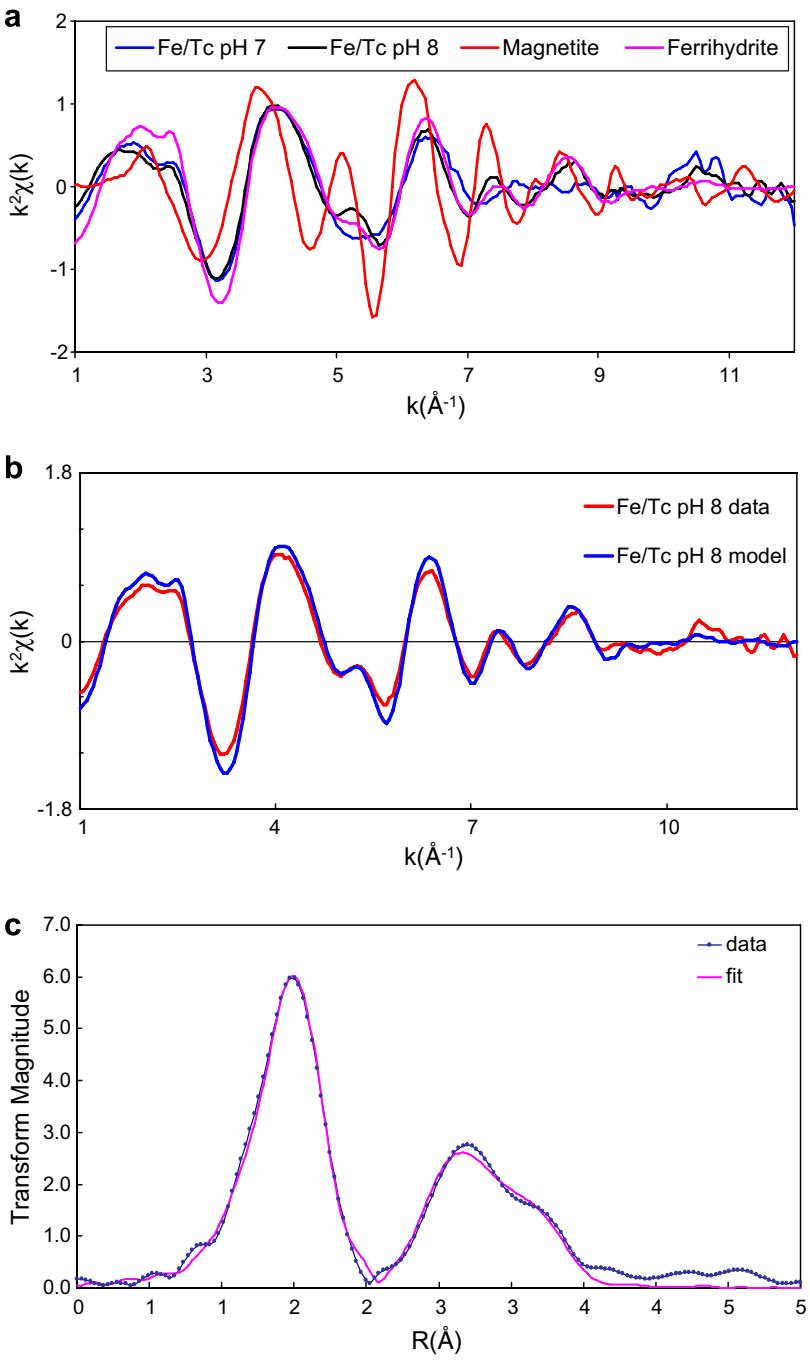

Fig. 9. (a) Fe-EXAFS [$\chi(k)$ data] of the pH 7 and pH 8 Fe/Tc precipitates as compared to magnetite and 6-line ferrihydrite, (b) linear combination modelling of the pH 8 $\chi(k)$ data using 11% magnetite and 89% ferrihydrite, and (c) radial transform of the Fe-EXAFS spectrum of 6-line ferrihydrite and results of fitting with the 2-Fe shell model.

feature of this model was a short Tc–Fe second shell bond similar to the short Tc–Tc bond in the amorphous $TcO_2{\cdot}nH_2O$ described by Lukens et al. (2002).

Application of this model to the pH 7 and pH 8 sample data produced fits that looked reasonable, but upon closer inspection there were problems. The Tc–Fe disorder was unreasonably large and the fit to the second transform peak was not ideal, especially in terms of phase. The model was consequently extended to allow for the formation of TcO_2 polymers (Vichot et al., 2002). These polymers could then coordinate to the ferrihydrite surface or vacancy sites. The main difference in this second model was a reduced contribution from Tc–Fe bonds, and the addition of Tc–Tc bonds. This alternative model was deemed plausible given the high Tc concentration in the precipitates.

In practice, it was found that fitting the second model was problematic since the EXAFS contribution from Tc–Fe and Tc–Tc were out of phase and nearly cancelled.

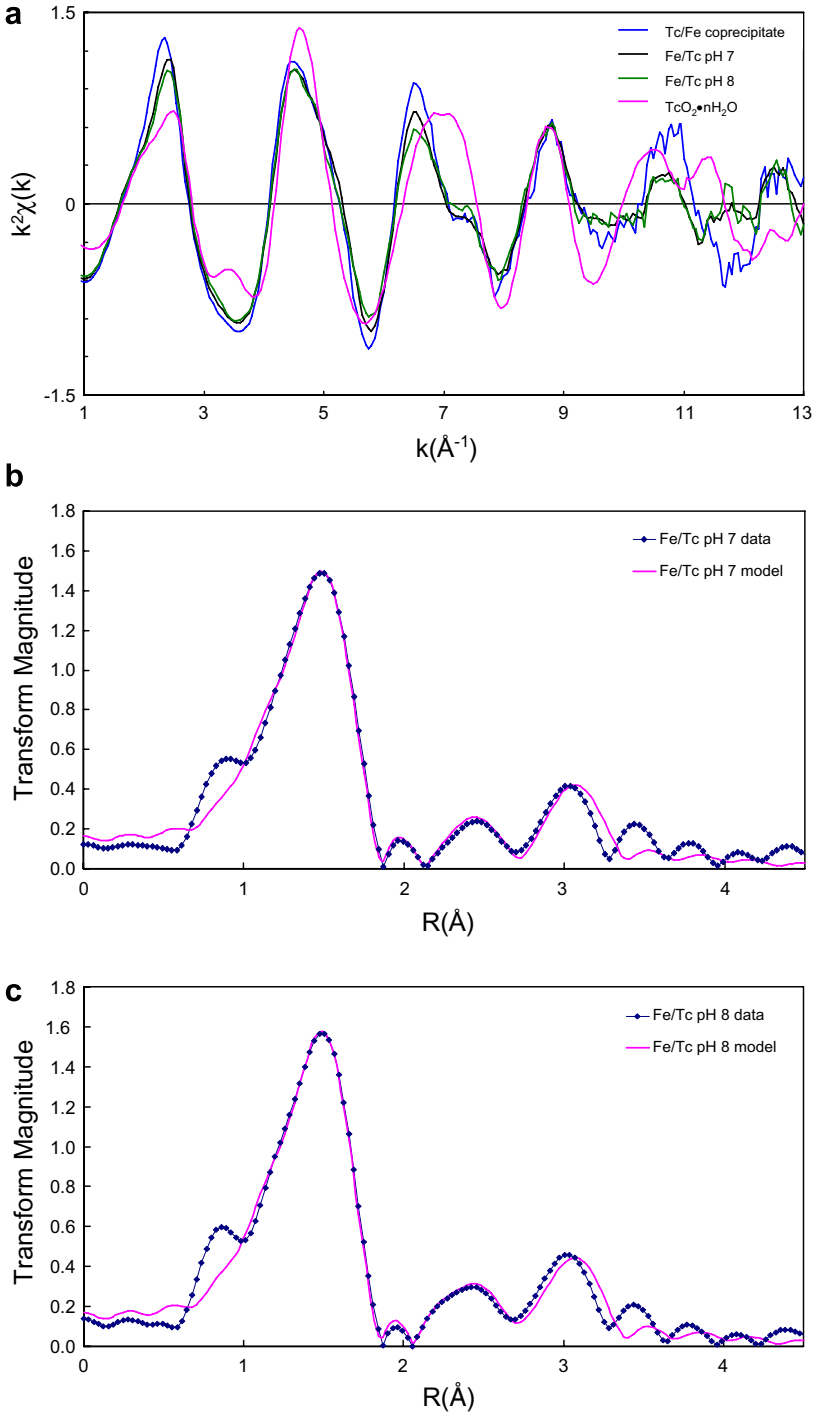

Fig. 10. (a) Tc-EXAFS [χ(k) data] of the pH 7 and pH 8 Fe/Tc precipitates as compared to $TcO_2{\cdot}nH_2O$ and Tc(IV)-coprecipitated with ferrihydrite, and (b) Fourier transform of the Fe/Tc pH 7 data and fitting results with the dimer model. (c) Fourier transform of the Fe/Tc pH 8 data and fitting results with the dimer model.

To constrain the fits, the Tc–Tc bond parameters were fixed at the values reported for the $TcO_2{\cdot}nH_2O$ solid (Lukens et al., 2002), and the number of Tc–Tc and Tc–Fe bonds were determined by the length of the Tc–Tc chains. For example, if the Tc chain length was two, each Tc on average would have one Tc neighbor, and 0.5 Fe neighbors.

The constrained polymer model produced good fits for the pH 7 and pH 8 samples (Fig. 10b and c) using reasonable parameters (Table 4). The model included an octahedral first shell, short Tc and Fe contributions constrained as discussed above, axial O neighbors from neighboring Fe and Tc octahedron, and a longer Fe bond. The multiple

Table 3
Ferrihydrite structural model derived from Fe-EXAFS fitting of 6-line ferrihydrite

Shell	N (fixed)	R (Å)	σ^2 (Å^2)
1st O short	3	1.92	0.0056
1st O long	3	2.06	0.0089
Fe short	3	2.99	0.0138
Fe long	3	3.45	0.0110
2nd O short	3	3.52	0.0099[a]
2nd O long	3	3.71	0.0099[a]

The fitting range was 2–13 Å^{-1} in k-space and 1–3.5 Å in r-space giving 17 possible independent parameters with 12 fitting parameters used in the model.
[a] Constrained to be equal.

Table 4
Results of fitting the Tc(IV) dimer model to the pH 7 and pH 8 Tc-EXAFS data

Shell	N	R (Å)	σ^2 (Å^2)
Tc/Fe pH 8			
1st O	6*	2.01 (0.01)	0.0065 (0.001)
Fe short	0.5 (0.1)	2.57 (0.02)	0.0014 (0.002)
Tc	1.0 (0.2)	2.57*	0.007*
2nd O short	2*	3.04 (0.04)	0.0034 (0.002)
Fe long	2*	3.50 (0.03)	0.0032 (0.002)
Tc/Fe pH 7			
1st O	6*	2.01 (0.01)	0.0065 (0.001)
Fe short	0.3 (0.1)	2.58 (0.02)	0.0008 (0.002)
Tc	1.3 (0.3)	2.57*	0.007*
2nd O short	2*	3.06 (0.04)	0.0082 (0.002)
Fe long	2*	3.50 (0.03)	0.0038 (0.002)

Parameters noted by * were fixed in the data fitting.

scattering parameters for paths within the Tc–O octahedron were determined from the corresponding single scattering paths and were not free parameters. The longer Fe bond was added to account for the extended Fe neighbors observed in the ferrihydrite structural model (Fig. 9c; Table 3) that influence the third Tc transform peak. Typically, the data range allowed for about 15 fitting parameters, but only 11 parameters were generally fit due to the imposed structural constraints. These fits were significantly better than with the single TcO_6 octahedron model, and, on average, indicated that the Tc polymers were approximately dimers (e.g., $N_{Tc} \sim 1$; Table 4).

3.3.3. Mössbauer spectroscopy

The wet chemical experiments (Figs. 2 and 3) were performed with isotopically enriched Fe(II) containing 96.7% ^{57}Fe, the Mössbauer active Fe isotope. This isotopic enrichment allowed Mössbauer measurements on the Fe/Tc precipitates in spite of their very low mass yield (e.g., <10 mg). Mössbauer measurements were performed on the precipitates from the pH 6.8, 7.0, and 8.0 experiments at 298, 77, and 12 K. The lowest temperature measurements did not yield essential information and are not reported here. The Mössbauer spectra of all three samples exhibited common aspects and only those from pH 7 and 8 are presented herein.

The room temperature spectra (RT, 298) of both samples were dominated by a doublet at 0–1.5 mm/s (Figs. 11 and 12a). The apparent Mössbauer parameters of the doublets were isomer shift (δ) = 0.4 mm/s and quadrupole splitting (Δ) = 0.6 mm/s. Doublets of this nature have been reported for ferrihydrite (Rancourt et al., 2005), superparamagnetic/nm-sized goethite (Murad and Cashion, 2004), magnetite (Goya et al., 2003), and maghemite (da Costa et al., 1998). The pH 8 sample also displayed two sextets in its RT spectrum (Fig. 11a; marked with t and o). The outer sextet (t) was due to Fe(III) in a tetrahedral coordination environment [$\delta = 0.32$ mm/s and quadrupole shift parameter (ε) = −0.15 mm/s, and hyperfine field (B_{hf}) = 47.5 Tesla (T)]. The inner sextet was consistent with a mixture of Fe(II) and Fe(III) in octahedral coordination ($\delta = 0.73$ mm/s and $\varepsilon = -0.06$ mm/s, and $B_{hf} = 43.5$ T). Consistent with SAED (Fig. 7a) and EXAFS fitting (Fig. 9b), this sextet pair indicated that a magnetite-like phase was present, although the observed B_{hf} for the tetrahedral (47.5 T) and octahedral (43.5 T) sites were slightly lower than pure magnetite [$t \sim 49$ T, $o \sim 46$ T; (Murad and Schwertmann, 1993)]. Moreover, the presence of discernable sextets for octahedral and tetrahedral sites at RT implied that the magnetite responsible for this spectral response was nominally >50 nm in size (Goya et al., 2003), although crystallites of this size were not noted by TEM. The RT spectral character and Mössbauer parameters for the pH 8 precipitate were similar to those observed for mineral products resulting from the reaction of $Fe^{2+}_{(aq)}$ with

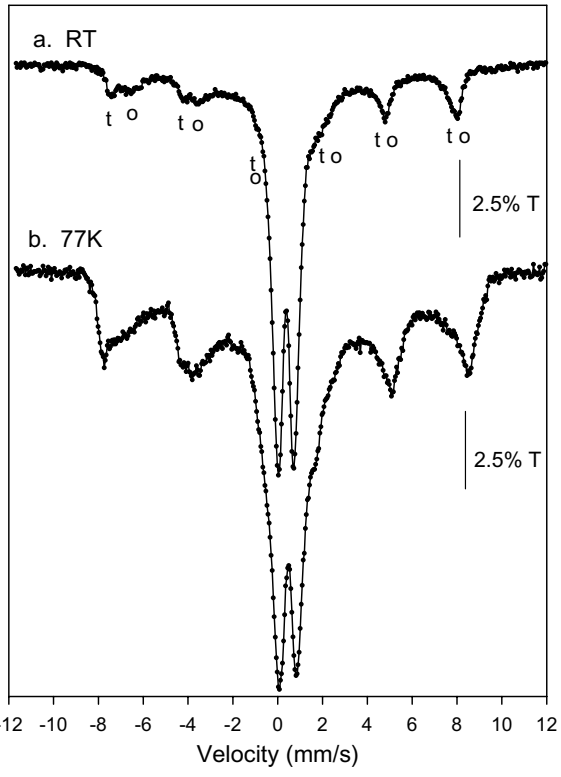

Fig. 11. ^{57}Fe transmission Mössbauer spectra of the pH 8, Fe/Tc precipitates: (a) room temperature (RT) and, (b) 77 K.

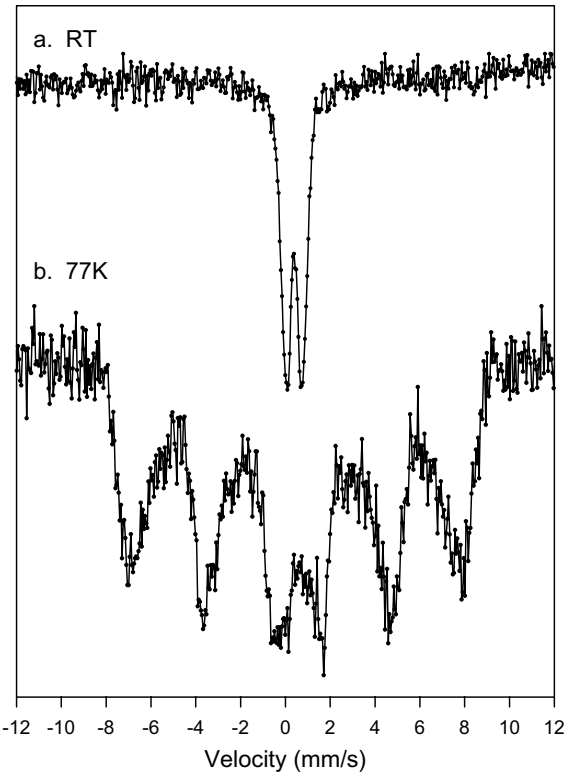

Fig. 12. ^{57}Fe transmission Mössbauer spectra of the pH 7, Fe/Tc precipitates: (a) room temperature (RT), and (b) 77 K.

ferrihydrite at alkaline pH with Fe(II)/Fe(III) = 0.15 (Jolivet et al., 1992).

Lowering the measurement temperature to 77 K reduced the spectral area of the central doublet in both samples (Fig. 11 and 12b). The doublet was completely eliminated at pH 7, where the precipitate displayed a magnetically ordered, partially collapsed sextet (Fig. 12b), consistent with the presence of a single phase. Recorded blocking temperatures (where 50% of the phase is magnetically ordered) for ferrihydrite, in contrast, range from 54 to 10.5 K depending on crystallite size and crystallinity (Murad et al., 1988; Murad and Cashion, 2004). An apparent blocking temperature of >77 K for the pH 7 redox product indicated the presence of a Fe(III) oxide with some difference in magnetic properties from ferrihydrite. Collectively, the RT and 77 K spectra of the pH 7 precipitate were virtually identical to those reported for 4 nm magnetite (Goya et al., 2003). The pH 8 precipitate also showed an increase in magnetic order at 77 K (Fig. 11b), albeit not as large as at pH 7, with enhanced spectral area associated with the sextet features observed at RT indicating thermal relaxation associated with magnetite particles that were nominally <10 nm in size (Goya et al., 2003).

The residual central doublet in the pH 8 sample at 77 K (Fig. 11b) could result from the presence of ferrihydrite or another, fine-grained Fe(III) oxide exhibiting superparamagnetic relaxation. Ferrihydrite was the most defensible choice given the Fe-EXAFS spectra and fitting results (Fig. 9b). The doublet was also observed at lower intensity in the 77 K spectrum of the pH 6.8 precipitate (data not shown), indicating the presence of ferrihydrite in this sample as well. Such features have not been observed in the 77 K Mössbauer spectrum of fine-grained stoichiometric magnetite (McNab et al., 1968; Gee et al., 2003; Goya et al., 2003) or fine-grained maghemite (da Costa et al., 1998). However, Jolivet et al. (1992) noted a similar Mössbauer spectra at 80 K for a 4.1 nm reaction product of Fe(II) with ferrihydrite. They speculated that this phase was a Fe(II)-induced transformation product of ferrihydrite that exhibited: (i) nascent spinel structure, (ii) poor long range order, and (iii) tetrahedral site vacancies. Their variable temperature measurements implied a blocking temperature for this phase of approximately 60 K, above that of ferrihydrite, and near that observed here.

3.4. Reaction of the Fe/Tc precipitates with molecular oxygen

The Fe/Tc particles characterized in Section 3.3 were subjected to oxidation in buffered suspensions that were bubbled with air at a rate that was sufficient to maintain oxygen saturation in the aqueous phase. The oxidation experiments were intended to provide additional, but indirect, evidence for the potential mode of Tc(IV) association with the Fe/Tc precipitate. It was hypothesized that adsorbed Tc(IV) would be oxidized and released rapidly, while the reaction of structural Tc(IV) would be slower and incomplete. The small masses of the Fe/Tc precipitates limited: (i) direct analyses of Fe(II) content by acid extraction, and (ii) long duration experiments.

3.4.1. Oxidative solubilization of Tc(VII)

The release of pertechnetate from the pH 6.8 and 7 precipitates showed an approximate linear increase with time (Fig. 13), consistent with pseudo-zero-order kinetics. Approximately 10% of the precipitated Tc(IV) was oxidized and released as Tc(VII) to the aqueous phase within 5 days. The small mass of Fe/Tc precipitate prevented further sampling past this time point. The pH 8 Fe/Tc precipitate showed a more rapid initial release (up to 4 h), followed by a period of significantly slower, linear dissolution kinetics. Only 7% of the precipitated Tc(IV) was oxidized and released from the pH 8 product over the course of 5 days of oxygen exposure. Dissolution rates were calculated from the slope of the linear portion of these plots (Table 5), and these ranged between 0.3 and 1.7 μmol Tc/g solid/h. The dissolution rates were ordered inversely with the buffered experimental pH values that applied during reaction and precipitation. The oxidation rate of Tc(IV) decreased with increasing Fe(II) concentration in the precipitate. Suspension pH was monitored during the oxidation of all four samples and it was found to be constant over the course of the experiments. These rates were significantly slower than the oxidation rate of fine-grained $TcO_2{\cdot}nH_2O$ (~11.9 μmol Tc/g solid/h) that was treated in the same manner where 67% of the precipitate dissolved in 4 days. The release of Tc(VII) from the Fe/Tc precipitates was significantly slower and less extensive then anticipated, given the oxidation/dissolution behaviour of $TcO_2{\cdot}nH_2O$. The results implied that Tc(IV) was protected against oxidation by structural incor-

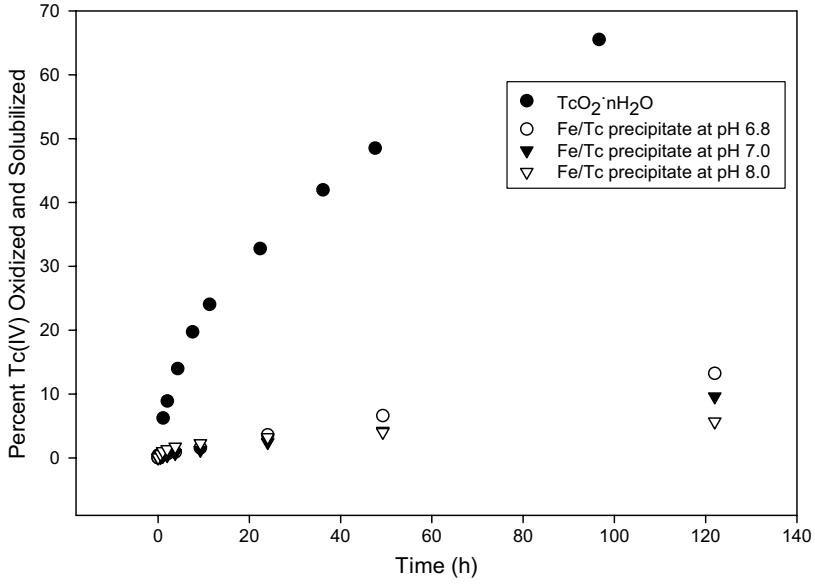

Fig. 13. Oxidative Tc(VII) release from Tc(IV)$O_2{\cdot}nH_2O$ and the pH 6.8, 7 and 8 Fe/Tc precipitates.

Table 5
Oxidative dissolution rate of Tc

pH	Solid concentration (mg/L)	Tc dissolution rate (μmol Tc/g solid/h)
6.8	2.95	1.7
7.0	3.88	1.3
8.0	11.32	0.3

poration or veneering by oxidized Fe in the Fe/Tc precipitates; or that oxidized Tc(IV) was unable to diffuse to the bulk aqueous phase from intracrystalline domains.

3.4.2. TEM analyses of the oxidized solids

The oxidized residues from the pH 6.8 and pH 7.0 Fe/Tc precipitates were similar in character. These, in turn, were similar to the pH 6.8 reduced material (Fig. 7), and were characterized by the presence of somatoidal or "needle-like" precipitates up to 50 nm long embedded in fine-grained material (Fig. 14). SAED of a 0.5 μm—diameter area of the pH 7 Fe/Tc precipitate (Fig. 7c) showed lines at 0.245, 0.215, 0.164, and 0.144 nm that were virtually identical to the unoxidized samples and that qualitatively equated with magnetite. There was no apparent global mineralogic change upon oxidation. EDS analysis of the somatoids and fine-grained materials in the pH 6.8 and 7.0 precipitates showed greater variability after oxidation, but no appreciable overall difference in composition from one another, averaging 85–88% atom Fe and 15–12% atom Tc. The observed Tc concentration in the solids changed little with oxidation.

The oxidized pH 8 Fe/Tc precipitates were comprised of ca 50–400 nm flat hexagonal crystals with closely associated fine-grained material that covered and connected the larger crystallites (Fig. 15). The hexagonal crystals yielded well-pronounced diffraction lines of 0.270 nm, the most intense diffraction maxima for hematite [$I(f) = 100$; $(hkl) = (104)$]. There was significant difference in the Fe:Tc ratio of the fine-grained material (88%:12%) as compared to the hexagonal crystallites (96–100%:4–0%), Fig. 15, based on EDS measurements performed with a 100 nm probe diameter. It appeared that some of the Tc signal from the hexagonal crystallites may have originated from fine-grained materials on their surface.

4. DISCUSSION

4.1. The reduction reaction

Our observations of homogeneous Tc(VII) reduction contrast with the experimental results of Cui and Eriksen (1996a) who found no homogeneous Tc(VII) reduction by $Fe(II)_{aq}$ at circumneutral pH. These authors contacted Tc(VII) (3.3×10^{-7} mol/L) with $Fe(II)_{TOT} = 5.8 \times 10^{-5}$ mol/L in glass reaction vessels at pH 7, and noted a significant reduction in pH (~1.5 units), $Fe(II)_{aq}$ (20.7%), and Tc(VII) (18%). Following this observation, they coated the interiors of their glass reaction vessels with hexadimethyldisilazane, and saw little change in $Fe(II)_{aq}$, Tc(VII), or pH under comparable experimental conditions; concluding that adsorbed Fe(II) to the glass vessel wall was the reductant in the early experiment.

Our experiments were not performed in coated glass, yet we observed no reduction of Tc(VII) at pH 7 with $Fe(II)_{aq} = 5.0 \times 10^{-5}$ mol/L over the time period of the Cui and Ericksen experiment (2750 min or 1.9 d; Fig. 3). Moreover we observed no glass discoloration later in the experiment that would result if adsorbed Fe(II) on vessel walls was oxidized by Tc(VII), and hydrolyzed and precipitated in place. We contend that the homogeneous reduction reaction is slow and promoted by hydrolyzed Fe(II) aqueous species as noted for Cr(VI) reduction. A measure of the reaction slowness can be gained by comparing our

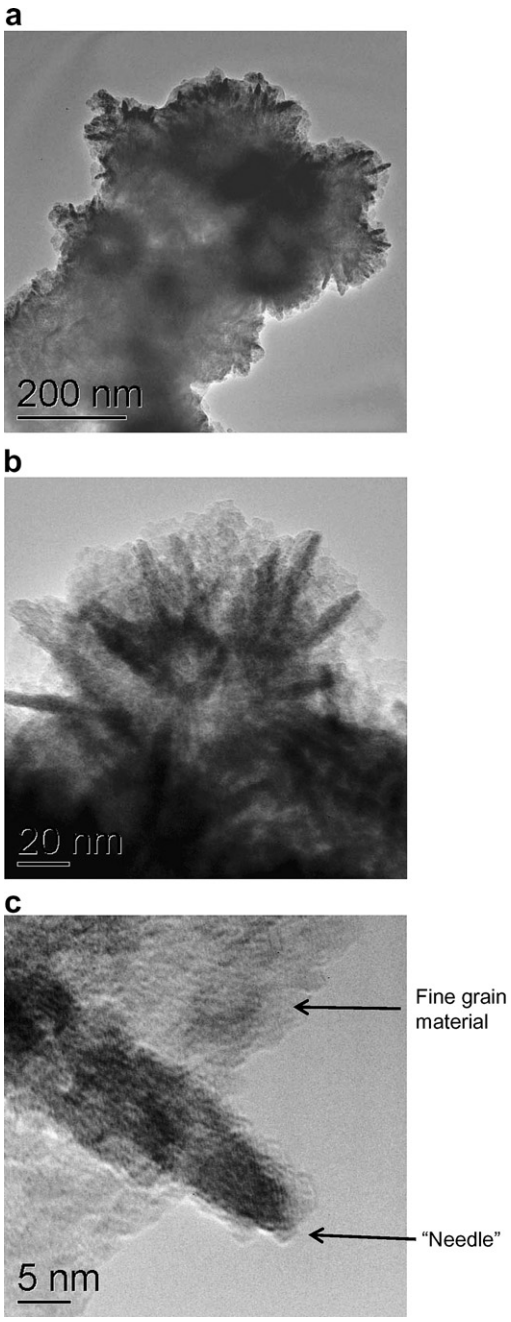

Fig. 14. Transmission electron micrographs (a–c) for the pH 7 Fe/Tc precipitate after 9.4 days of air oxidation.

rate of homogeneous Tc(VII) reduction as calculated at pH 7 with 0.05 mmol/L Fe(II) (e.g., $k_1 = 0.005$ day^{-1}) with the rate reported by Pettine et al. (1998) for $Cr(VI)O_4^{2-}$ reduction under comparable experimental conditions (e.g., pH ≈ 6.9–7.0 and $[Fe(II)_{aq}] \approx 0.04$ mmol/L). The ratio of reaction rates ($k_{1\text{-}Cr(VI)}/k_{1\text{-}Tc(VII)}$) was 2.5×10^4, underscoring the slow rate of homogeneous Tc(VII) reduction. This slow rate is a possible consequence of the very low redox potentials required for the one and two electron transfer reactions leading to the potential Tc(VI) (TcO_4^{2-}, $E° = -0.64$ V) and Tc(V) ($E° = -0.60$ V) intermediate species, that are unstable and disproportionate (Founta et al., 1987; Rard et al., 1999). Our observation of homogeneous reduction was enabled by higher Fe(II) concentrations (0.05–0.8 mmol/L) as compared to 0.0064–0.12 mmol/L by (Cui and Eriksen, 1996a), and longer reaction times (>14,000 h or 10 d).

The empirical observations of an increase in the apparent reduction rate of Tc(VII) with both Fe(II) concentration and pH were fully consistent with comparable observations made by Sedlak and Chan (1997) for Cr(VI). With regard to the pH effect, ferrous iron hydrolysis apparently decreases the activation energy for electron transfer and increases the electron density of the metal ion center to make it kinetically more reactive (Davies and Morgan, 1988; Wehrli, 1990; Stumm, 1992; Sedlak and Chan, 1997). However, there are major differences in the redox properties of the intermediate valence states of Cr and Tc that may affect their comparative kinetic behavior. Unlike Cr(VI), our homogeneous reduction data did not conform to a pseudo-first order model, as plots of $\ln[C_t/C_o]$ versus time showed curvilinear behaviour (e.g., increasing rate with reaction progress) even before the obvious onset of heterogeneous reduction (Fig. 4a). The acceleration in reduction, or autocatalysis by reaction intermediates or products, was believed to represent an evolution from homogeneous to heterogeneous reaction. Thus, the reaction domain was not classically homogeneous. The oxidation of $Fe(II)_{aq}$ by Tc(VII) yielded Fe(III) that hydrolyzed and quickly precipitated as a poorly crystalline oxyhydroxide because of its low solubility at circumneutral pH. A breakpoint between homogeneous and heterogeneous reduction was observed for four of the pH 7 experiments after the oxidation of 0.01–0.015 mmol/L of Fe(III), possibly signifying the presence of a threshold $Fe(III)_{aq}$ supersaturation value or Fe(III) oxide concentration for heterogeneous reduction. This concentration was approximately 100 times the solubility of ferrihydrite at this pH (Cornell and Schwertmann, 2000). It is possible that the interaction of Fe(II) and/or Tc(VII) with hydrolyzed Fe(III) clusters and other precursors of Fe(III) precipitates enhanced the kinetic reactivity of Fe(II) (and its hydrolyzed forms) with Tc(VII) during the "homogeneous phase".

Heterogeneous electron transfer promoted by sorbed Fe(II) was evident by a marked acceleration in Tc(VII) reduction rate that paralleled the observance of turbidity and Fe(III) precipitation in the batch reactors. Heterogeneous reduction appeared to be the primary observed process at higher Fe(II) concentrations and pH. Fe(II) is strongly absorbed by ferrihydrite and crystalline Fe(III) oxides (Jeon et al., 2003), and significant residual Fe(II) was observed in the Fe/Tc precipitates by Fe-XANES analyses (Fig. 8). Fe(II) sorption by Fe(II) oxides lowers the redox potential of Fe(II) (Silvester et al., 2005 and references therein), and concentrates Fe(II) to facilitate multi-electron redox reactions (Cui and Eriksen, 1996a; Amonette et al., 2000). In an unpublished study by our laboratory, we have observed very rapid Tc(VII) reduction by Fe(II) sorbed to hematite and goethite. Similarly, subsurface sediments with sorbed Fe(II) were effective reductants of Tc(VII) at circumneutral pH, displaying reaction half-lives ranging from

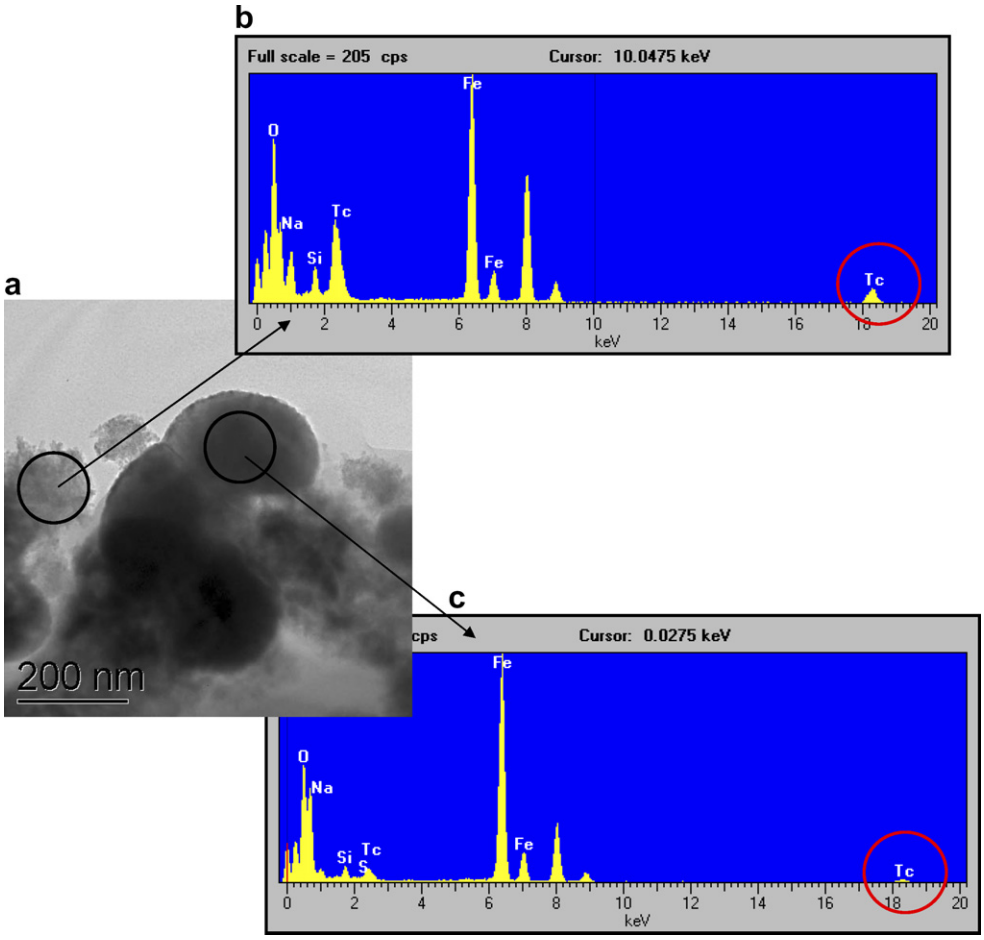

Fig. 15. Transmission electron micrograph (a) and energy dispersive spectroscopic analysis, (b) and, (c) of the pH 8 Fe/Tc precipitate after 9.4 days of air oxidation.

ca. 1 min to 3 h and with rates increasing with sorbed Fe(II) concentration (Fredrickson et al., 2004). The sediment displaying the most rapid heterogeneous reduction in this series (Eatontown) contained small crystallites of Fe(III) oxides. Moreover, magnetite, an apparent reaction product in these experiments, is also a strong heterogeneous reductant of Tc(VII) (Cui and Eriksen, 1996b; Lloyd et al., 2000).

4.2. Fe in the redox reaction product

The precipitates contained a mixture of Fe(II), Fe(III), and Tc(IV). Integrating the results of wet chemical, EDS, and XANES analyses yielded the following nominal compositions for the precipitates: (i) at pH 7—12.9% Fe(II), 72.9% Fe(III) and 14.2% Tc(IV), with $Fe_{TOT}/Tc(IV) = 6.04$, $Fe(III)/Tc(IV) = 5.13$, and $Fe(II)/Fe(III) = 0.18$, and (ii) at pH 8—21.7% Fe(II), 65.0% Fe(III), and 13.3% Tc(IV), with $Fe_{TOT}/Tc(IV) = 6.51$, $Fe(III)/Tc(IV) = 4.88$, and $Fe(II)/Fe(III) = 0.33$. The Fe(III)/Tc(IV) ratios for both precipitates were in excess of the stoichiometry (3) of the redox reaction (Eq. (3)), indicating uncertainty in the Fe valence quantification by XANES, or the post experiment oxidation of Fe(II). Tc XANES measurements, however, indicated no Tc(IV) oxidation, and for the purpose of further discussion we assume that the XANES-determined Fe(II)/Fe(III) ratios were representative of the redox product, while recognizing the unexplained disparity. Our observations of an Fe(II)-enriched redox product contrasted with those of Hansel et al. (2003a) and Wielinga et al. (2001), who observed no Fe(II) in Fe(III)/Cr(III) hydroxide precipitates resulting from $Cr(VI)O_4^{2-}$ reduction by biogenic $Fe(II)_{aq}$. Initial redox precipitates in their system exhibited a ferrihydrite-like structure and $Fe(III)/Cr(III) = 2.5$, slightly below the anticipated stoichiometry of 3.

The Fe/Tc solids exhibited ferrimagnetic behavior implying at least some conversion to magnetite. The presence of tetrahedral Fe-bonding as noted in the Fe-XANES spectra, the dual sextet Mössbauer pattern in the RT spectrum and results of Fe-EXAFS fitting for the pH 8 precipitate, and SAED d-spacings all supported the plausible presence of some magnetite. However, we cannot entirely discount the possibility that maghemite rather than magnetite was present, as these two phases are difficult to differentiate by X-ray diffraction, Mössbauer spectroscopy, and X-ray absorption spectroscopy because of their similar structure and possibility for solid solution formation (e.g., Hanzlik et al., 1996; McCormick and Adriaens, 2004;

Williams et al., 2005). The high angle (553) diffraction doublet (~89–91° 2θ) and several other low intensity diffraction peaks can allow discrimination between magnetite and maghemite (Daniels and Rosencwaig, 1969), but we did not have sufficient masses of the Fe/Tc precipitates to perform this analysis.

$Fe(II)_{aq}$ is very reactive with ferrihydrite at circumneutral pH (Cornell and Schwertmann, 2000; Zachara et al., 2002; Hansel et al., 2003b; Jeon et al., 2003; Pederson et al., 2005), the presumed initial redox product (e.g., Hansel et al., 2003a), and can induce its transformation to more crystalline phases such as goethite, hematite, and magnetite depending on the Fe(II)/Fe(III) ratio and pH (Jolivet et al., 1992; Tronc et al., 1992; Zachara et al., 2002; Hansel et al., 2003b; Pederson et al., 2005). However the high Fe(II)/Fe(III) ratio (1.5–24) in these experiments, which was determined by the initial $Fe(II)_{aq}$ and Tc(VII) concentrations, and the circumneutral to alkaline pH, placed the reaction product in the magnetite stability field. The observation of more magnetite in the pH 8 sample was consistent with its higher sorbed Fe(II) content and with past observations of conditions favoring magnetite formation.

The Fe/Tc redox products had a significantly lower Fe(II)/Fe(III) ratio (0.18–0.33) than stoichiometric magnetite (0.5). If all the Fe(II) in the reaction products were assumed to reside in stoichiometric magnetite [$Fe(II)Fe(III)_2O_4$], then 25% of the Fe in the pH 7 precipitate and 62% of the Fe in the pH 8 precipitate could reside in this phase (according to XANES analysis). However, the results of EXAFS fitting suggested far lower magnetite contents: 0% for pH 7 and 11% for pH 8. The presence of paired sextets in the pH 8 precipitate at RT (Fig. 8a), and infrequent SAED patterns consistent with crystalline magnetite (Fig. 7a) provided qualitative corroboration of EXAFS fitting results. More consistent with our observations was the presence of poorly ordered, Fe(II)-substituted ferrihydrite possibly representing protomagnetite. This phase exhibited diffuse electron diffraction rings signifying more disorder than 6-line ferrihydrite; perhaps it is of 2-line form.

In previous research on the biotransformation of ferrihydrite (Fredrickson et al., 1998), we noted formation of a black ferrimagnetic transformation product with magnetite-like Fe(II):Fe(III) stoichiometry that did not exhibit diffraction peaks of magnetite. Recent Fe-EXAFS measurements of a similar Fe(II)-enriched phase showed a ferrihydrite-like EXAFS spectrum almost identical to the pH 7 and pH 8 samples investigated here (data not shown). An Fe(II)-enriched ferrihydrite was also observed as an intermediate product in the bacterial transformation of ferrihydrite to green rust, and this phase exhibited a similar X-ray diffraction pattern to ferrihydrite (Kukkadapu et al., 2004). Apparently, ferrihydrite can incorporate significant Fe(II) without appreciably changing its disordered structural character. Ongoing research by our group seeks to clarify this unexpected behavior of ferrihydrite.

Most have observed that the reaction of Fe(II) with ferrihydrite at pH above neutrality yields magnetite as the primary product when Fe(II)/Fe(III) $\geqslant$ 0.5 (Sugimoto and Matijevic, 1980; Mann et al., 1989; Jolivet et al., 1992; Tronc et al., 1992). Because Fe(III) in our experiments was generated by kinetic reaction of Tc(VII) with $Fe(II)_{aq}$, the Fe(II)/Fe(III) ratio followed a complex temporal trajectory, and, for the pH 8 sample specifically, ranged from a nominally high value to one of 12 at experiment termination. Perhaps the incorporation of the large noted concentrations of Tc(IV) into the precipitate (ca. 12–15 atom %), in spite of its nearly equal ionic radii (0.645 Å) with Fe(III) (0.640 Å), inhibited the catalytic effect of Fe(II) on re-crystallization of the Fe(III) product (e.g., Pederson et al., 2005) and contributed to precipitate disorder. The coordination behavior of Tc(IV) apparently favors the formation of amorphous, rather than crystalline oxide solids at room temperature (Burnett et al., 1995; Rard et al., 1999; Lukens et al., 2002). Crystalline $Tc(IV)O_2$, however, adopts the rutile (TiO_2) structure (Rogers et al., 1969; Vichot et al., 2002). Titanium(IV) (0.68Å) substitutes widely in Fe(III) oxides (e.g., Fitzpatrick et al., 1978) and forms solid solution series in Fe(II)/Fe(III) spinels such as ulvospinel {Fe(II)[Fe(II)Ti(IV)]O_4} and in maghemite [Fe_2TiO_5; Lindsley (1976)]. Evidence was sought here, but not found, for the formation of comparable Tc(IV)-substituted, crystalline Fe(II)/Fe(III) oxides.

4.3. Tc in the redox reaction product

We had initially speculated that Tc(IV) would exist in a structural, co-precipitated molecular environment as defined by multiple second-shell Fe neighbors based on EXAFS analysis. This hypothesis was based on the belief that Tc(IV) and Fe(III) would precipitate in intimate association after either homogeneous or heterogeneous reaction. Given the known tendency of Tc(IV) to favor a hexacoordinate motif in aqueous complexes (Ben Said et al., 2000; Vichot et al., 2002) and crystalline solids (Rogers et al., 1969; Vichot et al., 2002), we further speculated that sorbed Tc(IV) would exist in an octahedral environment distributed within the Fe(III) oxide structure. In contrast, the best fit model to the Tc-EXAFS data was found to be a single $Tc(IV)_2O_{10}$ octahedral dimer linked in edge-sharing mode to a single Fe(III)–O octahedral site in ferrihydrite. This model was different from the extended $Tc(IV)O_2{\cdot}nH_2O$ octahedral chain model of Lukens et al. (2002) that described the structure of Tc(IV) products resulting from the reaction of Tc(VII) with a variety of environmental reductants including pyrite, magnetite, humic substances, and layer lattice silicates suspended in reducing groundwater (Maes et al., 2004). Their starting Tc(VII) concentrations (2.2×10^{-3} mol/L) however, were over 200 times larger then those used in the present experiments (1.1×10^{-5} mol/L).

The edge-sharing Tc(IV) dimer model was conceptually consistent with the formation of a polymeric surface complex along grain boundaries of individual nm-sized crystallites in larger particle aggregates, or at discontinuous point defects within disordered ferrihydrite. The approximate 15% atomic fraction of Tc(IV) in the precipitates could, marginally, be accommodated as a dimeric surface complex if the precipitated Fe(III) exhibited a site density comparable to rapidly precipitated hydrous ferric oxide

[$N_{s2} = 0.2$ mol/mol Fe; Dzombak and Morel (1990)]. The Fe-EXAFS spectrum of the reference 6-line ferrihydrite was best modeled with a site occupancy of 0.5, possibly indicating the presence of even more sites for incorporation of Tc(IV) dimers.

The predominant Tc(IV) aqueous species between pH 3 to 10 is reported to be $TcO(OH)_2^{o}{}_{(aq)}$ (Rard et al., 1999), which is thermodynamically equivalent to $Tc(OH)_4(H_2O)_2^{o}{}_{(aq)}$ (Rard et al., 1999; Ben Said et al., 2000). The molecular structure for this primary hydrolyzed species has been debated but not verified. A $Tc(OH)_4(H_2O)_2^{o}{}_{(aq)}$ complex would have structural analogy to the Lukens chain model but with equatorial OH groups replacing edge-shared oxygens. However, (Vichot et al., 2002) documented the presence of polymeric Tc(IV) species (with $N_{Tc} > 2$) at acidic pH with similar EXAFS signature to $Tc(IV)O_2{\cdot}nH_2O$, and speculated that these were precursors to precipitates. The formation of aqueous Tc(IV) dimers has also been suggested (Sundrehagen, 1979). Our structural model for the Fe/Tc precipitate may therefore be consistent with a neutral, dimeric surface complex, $(OH)_2(H_2O)_2Tc(O)_2(H_2O)_2Tc(O–)_{2(s)}$, where hydroxyls are in the equatorial plane of the distal Tc(IV) octahedron, waters are in the axial planes of both Tc(IV) octahedrons, oxygens bridge the equatorial plane between distal and proximate Tc(IV) centers, and equatorial oxygens (O–) in the proximate Tc(IV) octahedron are edge shared with Fe(III) in octahedral coordination.

The oxidation behavior of the precipitated Tc(IV) further suggested that its sorption state was not simply a surface complex on exposed surfaces of the ferrihydrite, but involved a more intimate association with internal domains of the precipitate. Its oxidation rate was significantly slower than $Tc(IV)O_2{\cdot}nH_2O$, suggesting that the dimeric complexes were in intra-aggregate domains or possibly unoccupied octahedral Fe(III) sites within individual crystallites that were restrictive to oxygen diffusion. XANES analyses of the oxidized precipitates showed a decreased Fe(II)/Tc(IV) ratio and lingering Tc(IV) in concentration equal to the unoxidized fraction. These intraparticle domains may have become further isolated from molecular oxygen through Fe(II) oxidation and Fe(III) precipitation in diffusion paths during the oxidation experiment, as increased Fe(II) in the precipitate was associated with a slower oxidation rate. The high Fe(II) content of the ferrihydrite may have functioned as an antioxidant for Tc(IV), with the resulting Fe(III) acting to further stabilize coordinated Tc(IV) in the Fe(III) oxide structure. Stabilized Tc(IV) apparently resided in the fine grained residual ferrihydrite, as TEM elemental analyses suggested that it did not incorporate into hematite that formed as an oxidation product in the pH 8 material (Fig. 15). Burke et al. (2006b) recently studied the oxidation of sediment-bound Tc(IV), implied by EXAFS analysis to be $TcO_2{\cdot}nH_2O$, that was formed by the reaction of Tc(VII) with biogenic Fe(II). These authors observed higher oxidation rates and extent for Tc(VII) then noted for our samples in Fig. 13, possibly reflecting the different molecular environments of Tc(IV) in the two materials as indicated by EXAFS measurements.

ACKNOWLEDGMENTS

This research was supported by the Environmental Remediation Sciences Program (ERSP), Office of Biological and Environmental Research (OBER), U.S. Department of Energy (DOE). The authors thank (i) Dr. Nancy Hess for commenting on the EXAFS analyses and the molecular forms of Tc(IV) hydrolysis species, and (ii) an anonymous reviewer made insightful comments on Tc reaction kinetics and intermediate species. Transmission electron microscopy and Mössbauer measurements were performed in the William R. Wiley Environmental Molecular Sciences Laboratory, a national scientific user facility sponsored by the Department of Energy's Office of Biological and Environmental Research and located at Pacific Northwest National Laboratory. PNNL is operated for the DOE by Battelle. Use of the Advanced Photon Source for XANES and EXAFS measurements was supported by the US DOE, Office of Science, under contract No. W-31-109-Eng-38.

REFERENCES

Allison J. D., Brown D. S., and Novo-Gradac, K. J. (1998) MINTEQA2/PRODEFA2, A Geochemical Assessment Model for Environmental Systems: User Manual Supplement for Version 4.0; U.S. Environmental Protection Agency: Washington, DC.

Amonette J. E., Workman D. J., Kennedy D. W., Fruchter J. S., and Gorby Y. A. (2000) Dechlorination of carbon tetrachloride by Fe(II) associated with goethite. *Environ. Sci. Technol.* **34**, 4606–4613.

Ben Said K., Fattahi M., Musikas C., Revel R., and Abbe J. C. (2000) The speciation of Tc(IV) in chloride solutions. *Radiochim. Acta* **88**, 567–571.

Bondietti E. A., and Francis C. W. (1979) Geologic migration potentials of Tc-99 and N-237. *Science* **203**, 1337–1340.

Buerge I. J., and Hug S. J. (1997) Kinetics and pH dependence of chromium(VI) reduction by iron(II). *Environ. Sci. Technol.* **31**, 1426–1432.

Burke I. T., Boothman C., Lloyd J. R., Mortimer R. J. G., Livens F. R., and Morris K. (2006a) Effects of progressive anoxia on the solubility of technetium in sediments. *Environ. Sci. Technol.* **39**, 4109–4116.

Burke I. T., Boothman C., Lloyd J. R., Livens F. R., Charnock J. M., McBeth J. M., Mortimer R. J. G., and Morris K. (2006b) Reoxidation behavior of technetium, iron, and sulfur inestuarine sediments. *Environ. Sci. Technol.* **40**, 3529–3535.

Burnett K. B., Campbell A. B., Jobe D. J., Lemire R. J., and Taylor P. (1995) Synthesis, characterization and heat of formation of the amorphous and crystalline forms of TcO_2. *Radiochim. Acta* **69**, 241–249.

Cornell R. M., and Schwertmann U. (2000) *The Iron Oxides: Structure, Properties, Reactions, Occurrences and Uses*. WILEY-VCH.

Cui D., and Eriksen T. E. (1996a) Reduction of pertechnetate by ferrous iron in solution: Influence of sorbed and precipitated Fe(II). *Environ. Sci. Technol.* **30**, 2259–2262.

Cui D., and Eriksen T. E. (1996b) Reduction of pertechnetate in solution by heterogeneous electron transfer from Fe(II)-containing geological material. *Environ. Sci. Technol.* **30**, 2263–2269.

da Costa G. M., De Grave E., and Vandenberghe R. E. (1998) Mössbauer studies of magnetite and Al-substituted maghemites. *Hyperfine Inter.* **117**, 207–243.

Daniels J. M., and Rosencwaig A. (1969) Mössbauer spectroscopy of stoichiometric and non-stoichiometric magnetite. *J. Phys. Chem. Solids* **30**, 1561–1571.

Davies S. H. R., and Morgan J. J. (1988) Manganese(II) oxidation kinetics on oxide surfaces. *J. Coll. Inter. Sci.* **129**(1), 63–77.

Drits V. A., Sakharov B. A., Salyn A. L., and Manceau A. (1993) Structural model for ferrihydrite. *Clay Miner.* **28**, 185–207.

Dzombak D. A., and Morel F. M. M. (1990) *Surface Complexation Modeling: Hydrous Ferric Oxides*. John Wiley.

Eary L. E., and Rai D. (1988) Chromate removal from aqueous wastes by reduction with ferrous ion. *Environ. Sci. Technol.* **22**, 972–977.

Eggleston R. A., and Fitzpatrick R. W. (1988) New data and a revised structural model for ferrihydrite. *Clays Clay Miner.* **36**(2), 111–124.

Eriksen, T. E. and Cui, D. (1991). *On the interaction of granite with Tc(IV) and Tc(VII) in aqueous solution*. SKB-TR-91-47. Swedish Nuclear Fuel and Waste Management Co., Stockholm.

Eriksen, T. E., Ndalamba, P., Cui, D., Bruno, J., Caceci, M., and Spahiu, K. (1993). *Solubility of the redox-sensitive radionuclides ^{99}Tc and ^{237}Np under reducing conditions in neutral to alkaline solution, effect of carbonate*. SKB-TR-93-18. Swedish Nuclear Fuel and Waste Management Co., Stockholm.

Fendorf S. E., and Li G. (1996) Kinetics of chromate reduction by ferrous iron. *Environ. Sci. Technol.* **30**, 1614–1617.

Fischer W. R., and Schwertmann U. (1974) The formation of hematite from amorphous iron(III)hydroxide. *Clays Clay Miner.* **23**, 33–37.

Fitzpatrick R. W., Le Roux J., and Schwertmann U. (1978) Amorphous and crystalline titanium and iron-titanium oxides in synthetic preparations, at near ambient conditions, and in soil clays. *Clays Clay Miner.* **26**(3), 189–201.

Founta A., Aikens D. A., and Clark H. M. (1987) Mechanism and kinetics of the stepwise voltammetric reduction of pertechnetate in alkaline solution to Tc(VI), Tc(V), and Tc(IV). *J. Electroanal. Chem.* **219**, 221–246.

Fredrickson J. K., Zachara J. M., Kennedy D. W., Dong H., Onstott T. C., Hinman N. W., and Li S. W. (1998) Biogenic iron mineralization accompanying the dissimilatory reduction of hydrous ferric oxide by a ground water bacterium. *Geochim. Cosmochim. Acta* **62**, 3239–3257.

Fredrickson J. K., Zachara J. M., Kennedy D. W., Kukkadapu R. K., McKinley J. P., Heald S. M., Liu C., and Plymale A. E. (2004) Reduction of TcO_4^- by sediment-associated biogenic Fe(II). *Geochim. Cosmochim. Acta* **68**(15), 3171–3187.

Gee S. H., Hong Y. K., Erickson D. W., and Park M. H. (2003) Synthesis and aging effect of spherical magnetite (Fe_3O_4) nanoparticles for biosensor applications. *J. Appl. Phys.* **93**(10), 7560–7562.

Goya G. F., Berquo T. S., Fonseca F. C., and Morales M. P. (2003) Static and dynamic magnetic properties of spherical magnetite nanoparticles. *J. Appl. Phys.* **94**(5), 3520–3528.

Hansel C. M., Wielinga B. W., and Fendorf S. (2003a) Structural and compositional evolution of Cr/Fe solids after indirect chromate reduction by dissimilatory iron-reducing bacteria. *Geochim. Cosmochim. Acta* **67**(3), 401–412.

Hansel C. M., Benner S. G., Neiss J., Dohnalkova A., Kukkadapu R. K., and Fendorf S. (2003b) Secondary mineralization pathways induced by dissimilatory iron reduction of ferrihydrite under advective flow. *Geochim. Cosmochim. Acta* **67**(16), 2977–2992.

Hanzlik M., Petersen N., Keller R., and Schmidbauer E. (1996) Electron microscopy and ^{57}Fe Mössbauer spectra of 10 nm particles, intermediate in composition between Fe_3O_4 and Fe_3O_3, produced by bacteria. *Geophys. Res. Lett.* **23**, 479–482.

Hess N. J., Yuanxian X., Rai D., and Conradson S. D. (2004) Thermodynamic model for the solubility of TcO_2xH_2O(am) in the Aqueous Tc(IV)–Na^+–Cl^-–H^+–OH^-–H_2O system. *J. Sol. Chem.* **33**(2), 199–226.

ICDD. (2003) *JCPDS Powder Diffraction Files, PDF*. International Centre for Diffraction Data.

Istok J. D., Senko J. M., Krumholz L. R., Watson D., Bogle M. A., Peacock A., Chang J.-Y., and White D. C. (2004) In situ bioreduction of technetium and uranium in a nitrate-contaminated aquifer. *Environ. Sci. Technol.* **38**, 468–475.

Janney D. E., Cowley J. M., and Buseck P. R. (2000a) Structure of synthetic 2-line ferrihydrite by electron nanodiffraction. *Amer. Mineral.* **85**, 1180–1187.

Janney D. E., Cowley J. M., and Buseck P. R. (2000b) Transmission electron microscopy of synthetic 2- and 6-line ferrihydrite. *Clays Clay Miner.* **48**, 111–119.

Jansen E., Kyek A., Schafer W., and Schwertmann U. (2002) The structure of six-line ferrihydrite. *Appl. Phys. A* **74**, S1004–S1006.

Jeon B.-H., Dempsey B. A., and Burgos W. D. (2003) Kinetics and mechanisms for reactions of Fe(II) with iron(III) oxides. *Environ. Sci. Technol.* **37**, 3309–3315.

Jeon B.-H., Dempsey B. A., Royer R. A., and Burgos W. D. (2004a) Low-temperature oxygen trap for maintaining strict anoxic conditions. *J. Environ. Eng. ASCE* **130**(11), 1407–1410.

Jeon B.-H., Kelly S. D., Kemner K. M., Barnett M. O., Burgos W. D., Dempsey B. A., and Roden E. E. (2004b) Microbial reduction of U(VI) at the solid–water interface. *Environ. Sci. Technol.* **38**(21), 5649–5655.

Jolivet J.-P., Belleville P., Tronc E., and Livage J. (1992) Influence of Fe(II) on the formation of the spinel iron oxide in alkaline medium. *Clays Clay Miner.* **40**(5), 531–539.

Kukkadapu R. K., Zachara J. M., Fredrickson J. K., and Kennedy D. W. (2004) Biotransformation of synthetic 2-line silica-ferrihydrite coprecipitates by a dissimilatory Fe(III)-reducing bacterium:, Formation of carbonate green rust in the presence of phosphate. *Geochim. Cosmochim. Acta* **67**, 1081–1087.

Lindsley D. H. (1976) The crystal chemistry and structure of oxide minerals as exemplified by the Fe–Ti oxides. In *Oxides Minerals, Reviews in Mineralogy 3* (ed. I. D. Rumble). Min. Soc. Am. Book Crafters, Inc., pp. L1–L60.

Liu C., Gorby Y. A., Zachara J. M., Fredrickson J. K., and Brown C. F. (2002) Reduction kinetics of Fe(III), Co(III), U(VI), Cr(VI), and Tc(VII) in cultures of dissimilatory metal-reducing bacteria. *Biotechnol. Bioeng.* **80**(6), 638–649.

Lloyd J. R., and Macaskie L. E. (1996) A novel phosphorimager-based technique for monitoring the microbial reduction of technetium. *Appl. Environ. Microbiol.* **62**(2), 578–582.

Lloyd J. R., Sole V. A., Van Praagh C. V. G., and Lovley D. R. (2000) Direct and Fe(II)-mediated reduction of technetium by Fe(III)-reducing bacteria. *Appl. Environ. Microbiol.* **66**(9), 3743–3749.

Lukens, Jr., W. W., Bucher J. J., Edelstein N. M., and Shuh D. K. (2002) Products of pertechnetate radiolysis in highly alkaline solution: structure of $TcO_2{\times}H_2O$. *Environ. Sci. Technol.* **36**, 1124–1129.

Maes A., Geraedts K., Bruggeman C., Vancluysen J., Rossberg A., and Hennig C. (2004) Evidence for the interaction of technetium colloids with humic substances by X-ray absorption spectroscopy. *Environ. Sci. Technol.* **38**, 2044–2051.

Mann S., Sparks N. H. C., Couling S. B., Larcombe M. C., and Frankel R. B. (1989) Crystallochemical characterization of magnetic spinels prepared from aqueous solution. *J. Chem. Soc., Faraday Trans. I* **85**(9), 3033–3044.

McCormick M. L., and Adriaens P. (2004) Carbon tetrachloride transformation on the surface of nanoscale biogenic magnetite particles. *Environ. Sci. Technol.* **38**, 1045–1053.

McNab T. K., Fox R. A., and Boyle A. J. F. (1968) Some magnetic properties of magnetite (Fe_3O_4) microcrystals. *J. Appl. Phys.* **39**(12), 5703–5711.

Meyer R. E., Arnold W. D., Case F. I., and O'Kelley G. D. (1991) Solubilities of Tc(IV) oxides. *Radiochim. Acta* **55**, 11–18.

Murad E., and Cashion J. (2004) *Mössbauer Spectroscopy of Environmental Materials and their Industrial Utilization*. Kluwer Academic Publishers, Dordrecht.

Murad E., and Schwertmann U. (1993) Temporal stability of a fine-grained magnetite. *Clays Clay Miner.* **41**(1), 111–113.

Murad E., Bowen L. H., Long G. J., and Quin T. G. (1988) The influence of crystallinity on magnetic ordering in natural ferrihydrites. *Clay Miner.* **23**, 161–173.

Pederson H. D., Postma D., Jakobsen R., and Larsen O. (2005) Fast transformation of iron oxyhydroxides by the catalytic action of aqueous Fe(II). *Geochim. Cosmochim. Acta* **69**(16), 3967–3977.

Pettine M., D'Ottone L., Campanella L., Millero F. J., and Passino R. (1998) The reduction of chromium(VI) by iron(II) in aqueous solutions. *Geochim. Cosmochim. Acta* **62**(9), 1509–1519.

Rancourt D. G., Thibault P.-J., Mavrocordatos D., and Lamarche G. (2005) Hydrous ferric oxide precipitation in the presence of nonmetabolizing bacteria: constraints on the mechanism of a biotic effect. *Geochim. Cosmochim. Acta* **69**(3), 553–577.

Rard J. A., Rand M. H., Anderegg G., and Wanner H. (1999) *Chemical Thermodynamics of Technetium*. Elsevier, Amsterdam.

Ravel B., and Newville M. (2005) ATHENA, ARTEMIS, HEPHAESTUS; data analysis for X-ray absorption spectroscopy using IFEFFIT. *J. Synchrotron Rad.* **12**(4), 537–541.

Rehr J. J., and Albers R. C. (2000) Theoretical approaches to X-ray absorption fine structure. *Rev. Mod. Phys.* **72**, 621–654.

Rogers D. B., Shannon R. D., Sleight A. W., and Gillson J. L. (1969) Crystal chemistry of metal dioxides with rutile-related structures. *Inorg. Chem.* **8**(4), 841–849.

Sass B. M., and Rai D. (1987) Solubility of amorphous chromium(III)–iron(III) hydroxide solid solutions. *Inorg. Chem.* **26**, 2228–2232.

Sedlak D. L., and Chan P. G. (1997) Reduction of hexavalent chromium by ferrous iron. *Geochim. Cosmochim. Acta* **61**(11), 2185–2192.

Silvester E., Charlet L., Tournassat C., Gehin A., Greneche J.-M., and Liger E. (2005) Redox potential measurements and Mossbauer spectrometry of Fe^{II} adsorbed onto Fe^{III} (oxy-hydr)oxides. *Geochim. Cosmochim. Acta* **69**(20), 4801–4815.

Stumm W. (1992) *Chemistry of the Solid–Water Interface: Processes at the Mineral–Water and Particle–Water Interface in Natural Systems*. John Wiley.

Sugimoto T., and Matijevic E. (1980) Formation of uniform spherical magnetite particles by crystallization from ferrous hydroxide gels. *J. Colloid Interf. Sci.* **74**(1), 227–243.

Sundrehagen E. (1979) Formation and hydrolysation of ^{99}Tc(IV). *Int. J. Appl. Radiat. Isot.* **30**, 739–749.

Tronc E., Belleville P., Jolivet J.-P., and Livage J. (1992) Transformation of ferric hydroxide into spinel by Fe^{II} adsorption. *Langmuir* **8**, 313–319.

Vichot L., Ouvrard G., Montavon G., Fattahi M., Musikas C., and Grambow B. (2002) XAS study of technetium(IV) polymer formation in mixed sulphate/chloride media. *Radiochim. Acta* **90**, 575–579.

Wehrli B. (1990) Redox reactions of metal ions at mineral surfaces. In *Aquatic Chemical Kinetics* (ed. W. Stumm). John Wiley, pp. 311–336.

Wielinga B. W., Mizuba M. M., Hansel C. M., and Fendorf S. (2001) Iron promoted reduction of chromate by dissimilatory iron-reducing bacteria. *Environ. Sci. Technol.* **35**, 522–527.

Wildung R. E., McFadden K. M., and Garland T. R. (1979) Technetium sources and behavior in the environment. *J. Environ. Qual.* **8**, 156–161.

Wildung R. E., Gorby Y. A., Krupka K. M., Hess N. J., Li S. W., Plymale A. E., McKinley J. P., and Fredrickson J. K. (2000) Effect of electron donor and solution chemistry on products of dissimilatory reduction of technetium by Shewanella putrefaciens. *Appl. Environ. Microb.* **66**(6), 2451–2460.

Wildung R. E., Li S. W., Murray C. J., Krupka K. M., Xie Y., Hess N. J., and Roden E. E. (2004) Technetium reduction in sediments of a shallow aquifer exhibiting dissimilatory iron reduction potential. *FEMS Microbiol. Ecol.* **49**, 151–162.

Williams A. G. B., and Scherer M. M. (2004) Spectroscopic evidence for Fe(II)–Fe(III) electron transfer at the iron oxide–water interface. *Environ. Sci. Technol.* **38**, 4782–4790.

Williams A. G. B., Gregory K. B. F. P. G., and Scherer M. M. (2005) Hexahydro-1,3,5-trinitro-1,3,5-triazine transformation by biologically reduced ferrihydrite: evolution of Fe mineralogy, surface area, and reaction rates. *Environ. Sci. Technol.* **39**, 5183–5189.

Zachara J. M., Kukkadapu R. K., Fredrickson J. K., Gorby Y. A., and Smith S. C. (2002) Biomineralization of poorly crystalline Fe(III) oxides by dissimilatory metal reducing bacteria (DMRB). *Geomicrobiol. J.* **19**(2), 179–207.

Zhao J., Huggins F. E., Feng Z., and Huffman G. P. (1994) Ferrihydrite: surface structure and its effects on phase transformations. *Clays Clay Miner.* **42**, 737–746.

Associate editor: George R. Helz